



HAL
open science

Quasi-thermal noise spectroscopy: The art and the practice

N. Meyer-Vernet, K. Issautier, M. Moncuquet

► **To cite this version:**

N. Meyer-Vernet, K. Issautier, M. Moncuquet. Quasi-thermal noise spectroscopy: The art and the practice. *Journal of Geophysical Research Space Physics*, 2017, 122 (8), pp.7925-7945. 10.1002/2017JA024449 . hal-01628354

HAL Id: hal-01628354

<https://hal.sorbonne-universite.fr/hal-01628354>

Submitted on 3 Nov 2017

HAL is a multi-disciplinary open access archive for the deposit and dissemination of scientific research documents, whether they are published or not. The documents may come from teaching and research institutions in France or abroad, or from public or private research centers.

L'archive ouverte pluridisciplinaire **HAL**, est destinée au dépôt et à la diffusion de documents scientifiques de niveau recherche, publiés ou non, émanant des établissements d'enseignement et de recherche français ou étrangers, des laboratoires publics ou privés.

¹ Quasi-thermal noise spectroscopy: the art and the ² practice¹

N. Meyer-Vernet,² K. Issautier², and M. Moncuquet²

Corresponding author: N. Meyer-Vernet, LESIA, Observatoire de Paris.
(nicole.meyer@obspm.fr)

¹Dedicated to the memory of Jean-Louis
Steinberg

²LESIA, Observatoire de Paris, PSL
Research University, CNRS, Sorbonne
Univ., UPMC, Univ. Paris Diderot,
Sorbonne Paris Cité, 92195 Meudon, France

received 8 Jun, 2017, accepted 22 Jul 2017

Key Points.

- We provide new calculations and analytical approximations for plasma measurements by QTN spectroscopy
- We study the compatibility with various space implementations and constraints
- We give some applications for future space missions

3 **Abstract.** Quasi-thermal noise spectroscopy is an efficient tool for mea-
4 suring in situ macroscopic plasma properties in space, using a passive wave
5 receiver at the ports of an electric antenna. This technique was pioneered
6 on spinning spacecraft carrying very long dipole antennas in the interplan-
7 etary medium - like ISEE-3 and Ulysses - whose geometry approached a “the-
8 oretician’s dream”. The technique has been extended to other instruments
9 in various types of plasmas onboard different spacecraft and will be imple-
10 mented on several missions in the near future. Such extensions require dif-
11 ferent theoretical modelizations, involving magnetized, drifting or dusty plas-
12 mas with various particle velocity distributions, and antennas being shorter,
13 biased or made of unequal wires. We give new analytical approximations of
14 the plasma quasi-thermal noise (QTN), and study how the constraints of the
15 real world in space can (or cannot) be compatible with plasma detection by
16 QTN spectroscopy. We consider applications to the missions Wind, Cassini,
17 Bepi-Colombo, Solar Orbiter and Parker Solar Probe.

1. Introduction

Thermal electromagnetic radiation, on which rely a large part of remote observations in astronomy and geophysics, is related to thermal fluctuations in radio-engineering circuits - the so-called Johnson noise - via the fluctuation-dissipation theorem. In the classical approximation, Nyquist's formula [Nyquist, 1928] tells us that a wave receiver in open circuit at the ports of an electric antenna immersed in black-body radiation of temperature T measures a voltage power spectrum

$$V_f^2 = 4k_B T R \quad (1)$$

where $hf \ll k_B T$ (h being the Planck constant) and $R = R_{EM}$ is the antenna radiation resistance (Figure 1, left). However most space missions involve electric antennas immersed in plasmas (Figure 1, right), where the quasi-thermal motion of electric charges produces electrostatic fluctuations generally exceeding the radiation electromagnetic field. In that case the main contribution to the measured power is the plasma quasi-thermal noise (QTN, Figure 2). This noise represents the long-wavelength measurement limit in radioastronomy [Meyer-Vernet *et al.*, 2000] and it has been suggested to play a major role in the production of non-thermal electrons in the solar wind ([Yoon *et al.*, 2016] and references therein).

In the ideal case of a plasma at equilibrium temperature T , this noise reduces to Nyquist's formula (1) with $R = R_P$, the antenna resistance resulting from the plasma thermal fluctuations. If the plasma is non-thermal, the noise is still fully determined by the particle velocity distributions provided it is stable [e.g., Sitenko, 1967; Fejer and Kan, 1969]. This result can be generalized to a magnetized plasma and enables one to

32 deduce the plasma properties from the measured voltage spectrum [*Meyer-Vernet, 1979*].
33 Since these electrostatic waves are significantly damped by the medium, the measured
34 plasma properties are local ones, so that QTN spectroscopy provides in situ measure-
35 ments [e.g., *Meyer-Vernet and Perche, 1989*], contrary to the usual spectroscopy based
36 on electromagnetic waves, which provides remote measurements.

37 This technique was pioneered aboard ISEE-3 which carried the most sensitive radio
38 receiver ever flown [*Knoll et al., 1978*]. Rather ironically, the paper which pioneered
39 the technique [*Meyer-Vernet, 1979*], submitted ten days before the ISEE-3 launch, was
40 in the process of being rejected on the grounds that the theory was too simple for being
41 applicable in the solar wind, when the data of the inboard radio receiver became available;
42 their agreement with the simple formulas proposed in the submitted manuscript prompted
43 its immediate acceptance. This paper also provided a logically satisfying explanation for
44 several observations previously interpreted as “new” emissions or instabilities, since “
45 *pluralitas non est ponenda sine necessitate*” [*Ockham, 1324*]; the QTN explanation was
46 soon confirmed by *Hoang et al. [1980]* and *Sentman et al. [1982]*.

47 The QTN measurement technique was subsequently used in various environments using
48 radio receivers that had similarly not been designed for that purpose [e.g., *Meyer-Vernet*
49 *et al., 1998*]. In particular for measuring on ISEE-3/ICE the electron density and tem-
50 perature in a comet’s tail [*Meyer-Vernet et al., 1986a, b*], where the electrons were too
51 cold for the inboard particle analyzer to measure them accurately. The QTN technique
52 was also used to measure the solar wind electron properties as a function of heliocentric
53 distance [*Hoang et al., 1992*] and outside the ecliptic on Ulysses [e.g., *Issautier et al.,*
54 *1998, 1999, 2008; Le Chat et al., 2011*], and at 1 AU on WIND [e.g., *Salem et al., 2001*;

55 *Issautier et al.*, 2005]. And also in planetary environments such as the Earth's outer
56 plasmasphere [*Lund et al.*, 1994], the Io plasma torus [e.g., *Meyer-Vernet et al.*, 1993;
57 *Moncuquet et al.*, 1995, 1997], and Saturn's magnetosphere [e.g., *Moncuquet et al.*, 2005;
58 *Schippers et al.*, 2013] using the RPWS experiment on Cassini [*Gurnett et al.*, 2004].

59 Why is the QTN technique so well adapted to measure the electron density and temper-
60 ature? There are four reasons for that. First of all, both properties are revealed in situ by
61 the location and broad spectral shape of the plasma frequency peak (see Figure 2), just
62 as traditional spectroscopy reveals the chemical composition and the temperature (albeit
63 remotely). Second, being passive, this instrument does not perturb the medium, contrary
64 to other wave techniques. Third, since it is based on electrostatic waves or fluctuations of
65 wavelength of the order or greater than the Debye length (or the electron gyroradius if the
66 plasma is strongly magnetised) and tending to infinity close to resonances, the technique
67 is equivalent to a detector of cross-section larger by several orders of magnitude than
68 that of classical detectors. And finally, for the same reason, it is relatively immune to
69 spacecraft photoelectrons and charging effects which affect traditional particle analyzers;
70 in particular, since the electron density is deduced from a spectral peak, this measure-
71 ment is independent on gain calibrations. Because of its reliability and accuracy, QTN
72 spectroscopy serves routinely to calibrate other instruments [e.g., *Maksimovic et al.*, 1995;
73 *Issautier et al.*, 2001; *Salem et al.*, 2001].

74 The drawback is that, contrary to the classical particle analysers, QTN spectroscopy
75 cannot measure directly the particle velocity distributions. Even though some moments
76 are revealed by spectral features (see Section 2), a full measurement requires solving an
77 inverse problem: modelise the electric antenna and the velocity distribution(s) with a

78 few parameters, calculate the corresponding QTN spectrum, and fitting the theory to the
79 data to determine the parameters of the distribution as sketched in Figure 2. In other
80 words, the QTN technique has the cons and pros of a global measurement: it measures
81 less parameters, but it can measure them faster and more accurately. Note, too, that
82 the technique is less adapted to measure the ions because they are revealed at lower
83 frequencies (Section 2.8) at which the spectrum can be spoiled by the shot noise.

84 This shot noise, produced by the fluctuations due to collection and emission of individual
85 electric charges by the antenna surface, can be a real nuisance for QTN spectroscopy. It is
86 very hard to modelize because, contrary to the QTN, it depends on the antenna floating
87 potential, which is badly known because the photoelectron and secondary emissions of
88 materials in space change significantly with ageing and have different properties from
89 those measured in the laboratory [e.g., *Kawasaki et al.*, 2016]. This shot noise is generally
90 negligible for wire dipole antennas around f_p [*Meyer-Vernet and Perche*, 1989], but this is
91 not so when the antennas are made of small spheres. Indeed, the shot noise is proportional
92 to the squared voltage produced by each charge collected or emitted ($\propto a^{-2}$ for spheres
93 of radius a since their capacitance $\propto a$), and to the events' rate - proportional to surface
94 area ($\propto a^2$), so that the variation with a cancels out. Therefore, the shot noise on spheres
95 does not decrease as their radius decreases, contrary to wires whose surface $\propto a$ whereas
96 the capacitance varies weakly with radius. This is the basic reason why spherical probes
97 are unadaptated for QTN spectroscopy, in addition to the fact that these probes must be
98 supported by difficult-to-modelize booms. For all these reasons, we will only consider wire
99 antennas in this paper, and will mention the shot noise only for estimating the extent to

100 which it may spoil QTN spectroscopy, in particular for fat or biased antennas (see Section
101 3.2).

102 Simple analytical approximations are invaluable for the preliminary design and inter-
103 pretation of space experiments. A number of such approximations were derived when
104 QTN spectroscopy was not yet a recognized technique and was used as a by-product of
105 radioastronomy experiments [*Meyer-Vernet and Perche*, 1989]. This technique will now
106 be implemented in the inner heliosphere by Solar Orbiter with shorter antennas [*Mak-*
107 *simovic et al.*, 2005; *Zouganelis et al.*, 2007], and with specifically designed instruments
108 in Mercury’s environment by Bepi-Colombo [*Moncuquet et al.*, 2006a] and in the solar
109 corona with Parker Solar Probe (PSP) [*Bale et al.*, 2016]. The properties of the wire
110 dipole antennas used in these missions are summarized in Table 1, together with those of
111 some previous missions; we do not include STEREO, whose antennas’ length is too short
112 for implementing QTN spectroscopy except in very high density structures [*Zouganelis et*
113 *al.*, 2010] (see Section 2.4).

114 This paper is organized as follows. Section 2 recalls the main properties of QTN under
115 different conditions and gives new analytical approximations having a wide range of appli-
116 cations, in particular for antennas of moderate length in non-thermal plasmas. Section 3
117 extends the calculations made for ideal cases (Figure 3) to antennas being unsymmetrical
118 or biased and to dusty plasmas. Unless otherwise stated, units are SI.

2. The Art

119 The basic shape of the QTN spectrum can be understood from simple plasma physics
120 [*Meyer-Vernet and Perche*, 1989]. Each charged particle passing by the antenna induces a
121 voltage pulse. This voltage is not Coulomb-like because the plasma particles are “dressed”

122 by their mutual coupling. At time scales corresponding to frequencies $f < f_p$, this dressing
 123 takes the simple form of a Debye sheath of scale L_D , the Debye length, so that each thermal
 124 electron produces on the antenna a voltage pulse of duration roughly equal to the time
 125 that it remains within a Debye length, i.e. about $1/(2\pi f_p)$; the Fourier transform of such
 126 a pulse is a constant for $f < f_p$, producing a plateau of amplitude determined by the bulk
 127 of the electrons. In contrast at higher frequencies, moving electrons excite plasma waves
 128 so that their dresses become more sophisticated [e.g., *Meyer-Vernet*, 1993], trailing long
 129 trains of Langmuir waves which produce the plasma frequency peak.

2.1. Basics

130 In the Vlasov framework, the plasma can be thought of as an assembly of independent
 131 test particles “dressed” by their collective interactions which determine the plasma dielec-
 132 tric permittivity defining the plasma spatial and temporal dispersion [*Rostoker*, 1961]. In
 133 the electrostatic limit ($\omega/kc \ll 1$, where $\omega = 2\pi f$ is the angular frequency, \mathbf{k} the wave
 134 vector and c the speed of light), the (linear) longitudinal ($\mathbf{E} \parallel \mathbf{k}$) electric field fluctuations
 135 in Fourier space are given from Poisson’s equation by [*Sitenko*, 1967]

$$\langle E^2(\mathbf{k}, \omega) \rangle = \frac{\langle \rho^2(\mathbf{k}, \omega) \rangle^{(0)}}{k^2 \epsilon_0^2 |\epsilon_L(\mathbf{k}, \omega)|^2} \quad (2)$$

136 where $\epsilon_L(\mathbf{k}, \omega)$ is the longitudinal dielectric function and $\langle \rho^2(\mathbf{k}, \omega) \rangle^{(0)}$ the free-space (test-
 137 particle) charge density fluctuations (in Fourier space) produced by quasi-thermal particle
 138 motions. In a weakly magnetized plasma ($\omega \gg \omega_g$, the electron angular gyrofrequency),
 139 the test particles can be assumed to move in straight lines, so that with a velocity distri-
 140 bution $f(\mathbf{v})$

$$\langle \rho^2(\mathbf{k}, \omega) \rangle^{(0)} = 2\pi e^2 \int d^3v f(\mathbf{v}) \delta(\omega - \mathbf{k} \cdot \mathbf{v}) \quad (3)$$

141 the particle number density being

$$n = \int d^3v f(\mathbf{v}) \quad (4)$$

142 In the presence of a magnetic field \mathbf{B} , the test particles follow helical orbits of (angular)

143 gyrofrequency ω_g , so that

$$\langle \rho^2(\mathbf{k}, \omega) \rangle^{(0)} = 2\pi e^2 \sum_{-\infty}^{\infty} \int d^3v f(\mathbf{v}) J_n^2(k_{\perp} v_{\perp} / \omega_g) \delta(\omega - n\omega_g - k_{\parallel} v_{\parallel}) \quad (5)$$

144 where v_{\parallel} and v_{\perp} are the velocity components respectively parallel and perpendicular to

145 \mathbf{B} and J_n are n^{th} order Bessel functions of the first kind [*Abramowitz and Stegun*, 1965].

146 With an electric antenna characterized by the current distribution $\mathbf{J}(\mathbf{k})$ in Fourier space,

147 immersed in a plasma drifting with velocity \mathbf{V} , the voltage power at the antenna ports at

148 frequency f is

$$V_f^2 = \frac{2}{(2\pi)^3} \int d^3k \frac{|\mathbf{k} \cdot \mathbf{J}|^2}{k^2} \langle E^2(\mathbf{k}, \omega - \mathbf{k} \cdot \mathbf{V}) \rangle \quad (6)$$

149 The power V_r^2 at the ports of a receiver of impedance Z_r is deduced from

$$V_r^2 / V_f^2 = |Z_r / (Z_r + Z_a)^2| \quad (7)$$

150 where Z_a is the antenna impedance.

2.2. Electric Antenna Response

151 For the simplest antenna, made of two aligned wires, each of length $L \ll \lambda$ and radius
 152 $a \ll [L_D, L]$ (Figure 1), the current distribution can be assumed to be triangular [Meyer
 153 and Vernet, 1974], so that

$$|\mathbf{k} \cdot \mathbf{J}| = \left| \frac{4 \sin^2(k_{\parallel} L/2)}{k_{\parallel} L} J_0(k_{\perp} a) \right| \quad (8)$$

154 where k_{\parallel} and k_{\perp} are the \mathbf{k} components respectively parallel and perpendicular to the
 155 antenna direction (see details in [Schiff, 1970; Couturier et al., 1981]). In most cases of
 156 interest, the wave numbers responsible for the noise are smaller than or of the order of
 157 the plasma Debye length (or the electron gyroradius if it is smaller), with $ka \ll 1$, so
 158 that $J_0(k_{\perp} a) \simeq 1$ except in very dense and cold plasmas as planetary ionospheres. An
 159 important consequence emerges from (8). Writing $k_{\parallel} L = kL \cos \alpha$ where α is the angle
 160 between \mathbf{k} and the antenna direction, one sees that whereas a short antenna ($kL \ll 1$)
 161 is mainly sensitive to \mathbf{k} parallel to the antenna ($\cos \alpha = 1$) as for electromagnetic waves,
 162 on the contrary a long antenna ($kL \gg 1$) is mainly sensitive to wave vectors roughly
 163 perpendicular to its proper direction [Meyer-Vernet, 1994].

164 If the plasma fluctuations are isotropic in the antenna frame (which holds with $V = 0$
 165 and an isotropic velocity distribution in a weakly magnetized plasma), (6) becomes

$$V_f^2 = \frac{8}{\pi^2} \int_0^{\infty} dk F(kL) \langle E^2(k, \omega) \rangle \quad (9)$$

166 with

$$F(x) = 1/(32\pi) \int d\Omega |\mathbf{k} \cdot \mathbf{J}|^2 = [\text{Si}(x) - \text{Si}(2x)/2 - 2 \sin^4(x/2)/x] J_0^2(xa/L)/x \quad (10)$$

167 where $\text{Si}(x) = \int_0^x dt \sin t/t$ is the sine integral function [Abramowitz and Stegun, 1965].

168 Two approximations are useful:

$$F(x) \simeq x^2/24 \quad \text{for } x < 1 \quad (11)$$

$$F(x) \simeq \pi/(4x) \quad \text{for } x \gg 1 \quad (12)$$

169 with (11) approximating (10) better than 5% when $x \lesssim 1$.

170 When the plasma fluctuations are anisotropic with a symmetry axis (for example with
171 a drift of velocity \mathbf{V} or a static magnetic field \mathbf{B}), a different simplification arises. Since
172 in that case the electric fluctuations are independent of the azimuthal angle ϕ around the
173 symmetry axis, (6) can be calculated as

$$V_f^2 = \frac{1}{2\pi^2} \int_0^\infty dk \int_0^\pi \sin \theta d\theta \langle E^2(k, \theta, \omega - k \cdot V \cos \theta) \rangle \int_0^{2\pi} \frac{d\phi}{2\pi} |\mathbf{k} \cdot \mathbf{J}|^2 \quad (13)$$

174 where θ is the angle between \mathbf{k} and the symmetry axis and (8) yields

$$\int_0^{2\pi} \frac{d\phi}{2\pi} |\mathbf{k} \cdot \mathbf{J}|^2 = \frac{8}{\pi} \int_0^{2\pi} d\phi \frac{\sin^4(kL \cos \alpha/2)}{(kL \cos \alpha)^2} J_0^2(ka \sin \alpha) \quad (14)$$

175 α being the angle between \mathbf{k} and the antenna direction, given by

$$\cos \alpha = \cos \theta \cos \beta + \sin \theta \sin \beta \cos \phi \quad (15)$$

176 where β is the angle between the antenna and the symmetry axis.

177 If the antenna is parallel to the symmetry axis ($\beta = 0$), the QTN is given by (13) with
 178 from (8)

$$\int_0^{2\pi} \frac{d\phi}{2\pi} |\mathbf{k} \cdot \mathbf{J}|^2 = \left[\frac{4 \sin^2(kL \cos \theta/2)}{|kL \cos \theta|} J_0(ka \sin \theta) \right]^2 \quad (16)$$

179 On the other hand, if the antenna is perpendicular to the symmetry axis ($\beta = \pi/2$), (15)
 180 reduces to $\cos \alpha = \sin \theta \cos \phi$, so that with the change of variable $s = kL \sin \theta \cos \phi$ in the
 181 integral (14), we find

$$\int_0^{2\pi} \frac{d\phi}{2\pi} |\mathbf{k} \cdot \mathbf{J}|^2 = F_{\perp}(kL \sin \theta)/2 \quad (17)$$

$$F_{\perp}(x) = \frac{64}{\pi} \int_0^x ds \frac{\sin^4(s/2)}{s^2(x^2 - s^2)^{1/2}} \quad (18)$$

$$= \frac{8}{x} \left[2 \int_0^x dt J_0(t) - \int_0^{2x} dt J_0(t) + J_1(2x) - 2J_1(x) \right] \quad (19)$$

182 where we have assumed $ka \ll 1$. Equation (19) yields $F_{\perp}(x) \simeq x^2$ for $x < 1$, and
 183 $F_{\perp}(x) \simeq 8/x$ for $x \gg 1$.

184 The antenna response $F_{\perp}(x)$, given by (18)-(19) with $x = kL \sin \theta \sin \beta$, is also relevant
 185 whatever the antenna direction in a particular case: \mathbf{k} roughly perpendicular to the sym-
 186 metry axis. Therefore the function F_{\perp} was used both for calculating the quasi-thermal
 187 noise in Bernstein waves [*Meyer-Vernet et al.*, 1993; *Moncuquet et al.*, 1995] (see Section
 188 2.4) and the Doppler-shifted quasi-thermal noise of ions [*Issautier et al.*, 1999] (see Section
 189 2.8).

2.3. Dealing with Non-Maxwellians: Generalized Temperatures

190 Non-maxwellian velocity distributions are ubiquitous in space plasmas. The culprits
 191 are Coulomb collisions, whose cross-section decreases as the inverse square of the particle

192 energy, so that, even when the bulk of the distribution is dominated by collisions, the faster
 193 particles are not, making suprathermal tails ubiquitous [e.g., *Scudder and Olbert, 1979;*
 194 *Scudder and Karimabadi, 2013*]. Contrary to Maxwellians which are completely defined
 195 by two parameters (density and temperature), non-thermal distributions raise a major
 196 problem for measuring devices because their full characterization may need an infinite
 197 number of parameters. Indeed, sixty years after the beginning of the space age, nobody
 198 knows the accurate shape of particle velocity distributions in space. This is especially
 199 true for electrons, which either cannot be detected at energies (in eV) smaller than the
 200 absolute value of the spacecraft potential if it is negative - as occurs in inner planetary
 201 magnetospheres, or are strongly perturbed by this potential and by photoelectrons if it is
 202 positive - as occurs in the solar wind [e.g., *Garrett, 1981; Whipple, 1981*].

203 Still worse, in the absence of equilibrium, the “temperature” revealed by instruments
 204 generally depends on the measured energy range. In order to derive generic results, it is
 205 useful to characterize an isotropic non-maxwellian velocity distribution, depending on the
 206 speed v , by its generalized temperatures defined as [*Meyer-Vernet, 2001*]

$$k_B T_q / m = (\langle v^q \rangle / c_q)^{2/q} \quad (20)$$

$$c_q = (q + 1)!! \quad \text{for } q \text{ even} \quad (21)$$

$$c_q = \frac{2^{1+q/2}}{\pi^{1/2}} \left(\frac{q + 1}{2} \right)! \quad \text{for } q \text{ odd} \quad (22)$$

207 where $q > -3$ is an integer, m is the electron mass, k_B is Boltzmann’s constant, and the
 208 scalar moment of order q is

$$\langle v^q \rangle = \int d^3v v^q f(\mathbf{v})/n \quad (23)$$

209 The coefficients c_q are defined so that if the distribution is Maxwellian, all T_q 's are equal
 210 to its classical temperature. The smaller the index q , the slower the particles responsible
 211 for T_q , and for velocity distributions having a suprathermal tail, the smaller the value of
 212 T_q . In particular

$$T_2 = m\langle v^2 \rangle / (3k_B) \equiv T \quad (24)$$

213 is the classical kinetic temperature, T_1 is related to the mean random speed $\langle v \rangle$ as

$$\langle v \rangle = [8k_B T_1 / (\pi m)]^{1/2} \quad (25)$$

214 and T_{-2} is related to the Debye length L_D as

$$L_D = [\epsilon_0 k_B T_{-2} / (n e^2)]^{1/2} \quad (26)$$

215 Therefore an instrument detecting essentially the low-energy particles (which determine
 216 the Debye length), will find, if a Maxwellian is assumed, a temperature close to T_{-2} ,
 217 whereas an instrument measuring the flux will find a temperature close to T_1 . It is there-
 218 fore not surprising that a number of temperature measurements in which a Maxwellian
 219 is assumed are inconsistent, so that new methods are being devised ([e.g., *Dudík et al.*,
 220 2017] and references therein).

221 The simplest way of representing a distribution having a supra-thermal tail is the so-
 222 called kappa distribution [*Vasyliunas*, 1968], which can be written

$$f_{\kappa}(v) \propto [1 + v^2/(\kappa v_0^2)]^{-(\kappa+1)} \quad (27)$$

223 and has been used for modelling the QTN by *Chateau and Meyer-Vernet* [1991]; *Zouganelis*
 224 *et al.* [2008]; *Le Chat et al.* [2009]. Since the probability for the speed to lie in the range
 225 $[v, v + dv]$ is $f_{\kappa}(v) \times 4\pi v^2 dv$ and we have $[\frac{d}{dv}[v^2 f_{\kappa}(v)]]_{v=v_0} = 0$, the most probable speed
 226 equals v_0 . The greater the value of κ , the closer is the distribution to a Maxwellian, with
 227 $f_{\kappa}(v) \rightarrow e^{-v^2/v_0^2}$ when $\kappa \rightarrow \infty$.

228 At low speeds, developing (27) in series yields $f_{\kappa}(v) \propto 1 - (1 + 1/\kappa)v^2/v_0^2$; hence the
 229 Kappa distribution decreases faster with v than the Maxwellian $e^{-v^2/v_0^2} \propto 1 - v^2/v_0^2$. In
 230 contrast, at high speeds $f_{\kappa}(v) \propto (v^2/\kappa v_0^2)^{-(\kappa+1)}$; hence the Kappa distribution decreases
 231 slower than a Maxwellian. This illustrates an interesting property of Kappa distributions.
 232 Whereas at low speeds, a Kappa can be fitted by a Maxwellian of temperature smaller
 233 than its actual kinetic temperature, its high speed power-law decrease can mimic (albeit in
 234 a narrow energy range) a Maxwellian of much higher temperature. Taking these two faces
 235 into account can resolve a number of apparent contradictions arising when observations
 236 are interpreted with tools that assume Maxwellian distributions [e.g., *Nicholls et al.*, 2012].

237 With a Kappa distribution (27), we find from (20)

$$T_2 = (mv_0^2/2k_B)\kappa/(\kappa - 3/2) \equiv T \quad (28)$$

$$T_1 = T \times (\kappa - 3/2) [\Gamma(\kappa - 1)/\Gamma(\kappa - 1/2)]^2 \quad (29)$$

$$T_{-1} = T \times (\kappa - 3/2) [\Gamma(\kappa - 1/2)/\Gamma(\kappa)]^2 \quad (30)$$

$$T_{-2} = T \times (\kappa - 3/2)/(\kappa - 1/2) \quad (31)$$

For example with $\kappa = 4$, we have $T_{-1} \simeq 0.77 \times T$ and $T_{-2} \simeq 0.71 \times T$. From (28), a finite value of the kinetic energy requires $\kappa > 3/2$. On the other hand, the Debye length is given by (26), (28), and (31) as [Chateau and Meyer-Vernet, 1991]

$$L_D = \frac{v_0}{\omega_p} \left[\frac{\kappa}{2\kappa - 1} \right]^{1/2} \quad (32)$$

suggesting that the Debye screening has a normal behavior even when κ approaches $3/2$, despite some arguments to the contrary [e.g., Fahr and Heyl, 2016].

Another popular representation of non-thermal distributions is the sum of a cold (“core”) and a hot maxwellian of respective density and temperature n_c , n_h , T_c , T_h , which has one more free parameter than the Kappa distribution. In that case we have $T \equiv T_2 = (n_c T_c + n_h T_h)/(n_c + n_h)$, whereas $T_{-1} = T_c(n_c + n_h)^2/[n_c + n_h(T_c/T_h)^{1/2}]^2$ and $T_{-2} = (n_c + n_h)/(n_c/T_c + n_h/T_h)$; hence with a dilute hot maxwellian ($n_h/n_c \ll 1$, $T_h/T_c \gg 1$), we have $T_{-1} \simeq T_{-2} \simeq T_c$, the core temperature.

A further popular representation is the sum of a cold Maxwellian (of temperature T_c) containing the bulk of the distribution plus a hot Kappa distribution. Indeed, low-energy particles are generally collisional whereas faster ones are not, and many processes - including the spontaneously emitted Langmuir waves, i.e. the QTN [e.g., Yoon, 2014; Yoon *et al.*, 2016] - tend to generate Kappa distributions via non-linearities. In that case, we have as previously $T_{-1} \simeq T_{-2} \simeq T_c$.

2.4. Core Electron Temperature

As noted above, in a weakly magnetized plasma, the electron QTN spectrum exhibits a generic low-frequency plateau which is produced by electrons passing-by the antenna. This suggests that the plateau will mainly reveal the temperature defining the Debye length.

258 We derive below a generic expression of this plateau, relevant for a number of space
 259 radio instruments and independent of the detailed shape of the distribution, provided it
 260 is isotropic.

261 In a weakly magnetized plasma with an isotropic electron velocity distribution, (3)
 262 reduces to

$$\langle \rho^2(\mathbf{k}, \omega) \rangle^{(0)} = \frac{(2\pi e)^2}{k} \int_{\omega/k}^{\infty} dv v f(v) \quad (33)$$

263 which yields for $\omega/kv \ll 1$

$$\langle \rho^2(\mathbf{k}, \omega) \rangle^{(0)} \simeq \frac{\pi e^2}{k} n \langle v^{-1} \rangle \quad (34)$$

264 In the same limit, we have

$$\epsilon_L \simeq 1 + \omega_p^2 \langle v^{-2} \rangle / k^2 \equiv 1 + 1/(k^2 L_D^2) \quad (35)$$

265 with L_D given by (26). For a wire antenna (Figure 1), Eqs.(2), (9), (34) and (35) yield

$$V_f^2 \simeq \left(\frac{2^7 m k_B T_{-2}^2}{\pi^3 \epsilon_0^2 T_{-1}} \right)^{1/2} F_0(L/L_D) \quad (36)$$

$$F_0(t) = \int_0^{\infty} dy \frac{y F(yt)}{(1+y^2)^2} \quad (37)$$

266 $F(x)$ being given by (10). The function $F_0(L/L_D)$ is shown in Figure 4. The simple
 267 expression (36) of the plateau level is generic since it holds whatever the ratio L/L_D and
 268 the shape of the (isotropic) electron velocity distribution.

For $L/L_D \gg 1$, $F(x)$ can be approximated by (12), so that (37) yields

$$F_0(L/L_D) \simeq (\pi^2/16)L_D/L \quad \text{for } L/L_D \gg 1 \quad (38)$$

whence from (36)

$$V_f^2 \simeq \frac{(\pi/2)^{1/2} k_B T_{-2}^{3/2}}{\epsilon_0 \omega_p L T_{-1}^{1/2}} \simeq \frac{3.5 \times 10^{-14} T_{-2}^{3/2}}{n^{1/2} L T_{-1}^{1/2}} \quad \text{for } L/L_D \gg 1 \quad (39)$$

269 equivalent to a result by *Chateau and Meyer-Vernet* [1991]. One sees on Figure 4 that
 270 the approximation (38) (dashed red line), yielding (39), only holds for extremely long
 271 antennas. In practice, however, one expects $L/L_D \sim 2.5 - 6$ for Bepi-Colombo and
 272 $L/L_D \sim 1 - 2.5$ for Solar Orbiter in the solar wind at 0.3 AU., whereas for Parker Solar
 273 Probe at 10 solar radii we have $L/L_D \sim 2 - 3$.

274 In these cases, a much better approximation can be derived. Indeed, for $2 \lesssim L/L_D \lesssim 7$,
 275 (37) yields $F_0 \simeq 0.05$ within 10% (solid red line in Figure 4), which yields

$$V_f^2 \simeq \frac{1}{\pi^2 \epsilon_0} \left[\frac{m k_B T_{-2}^2}{T_{-1}} \right]^{1/2} \simeq 4.07 \times 10^{-17} \frac{T_{-2}}{T_{-1}^{1/2}} \quad \text{for } 2 \lesssim L/L_D \lesssim 7 \quad (40)$$

276 With a roughly maxwellian core of temperature T_c and a dilute halo, we have $T_{-2}/T_{-1}^{1/2} \simeq$
 277 $T_c^{1/2}$, whence

$$V_f^2 \simeq 4.07 \times 10^{-17} T_c^{1/2} \quad \text{for } 2 \lesssim L/L_D \lesssim 7 \quad (41)$$

278 Note that with a Kappa distribution we have

$$\frac{T_{-2}}{T_{-1}^{1/2}} = T^{1/2} \frac{(\kappa - 3/2)^{1/2} \Gamma(\kappa)}{\Gamma(\kappa + 1/2)} \quad (42)$$

279 yielding $T_{-2}^2/T_{-1} \simeq 0.66 \times T \simeq 0.93 \times T_{-2}$ for $\kappa = 4$, so that the temperature measured via
 280 the plateau level is close to that defining the Debye length, similar to a ‘‘core’’ temperature.

281 However with $\kappa = 2$, we have $T_{-2}^2/T_{-1} \simeq 0.85 \times T_{-2}$, so that in that case, the plateau

282 yields a temperature smaller than the “core” temperature T_{-2} by about 15%; this reflects
 283 the shortage of low-energy particles for kappa distributions with respect to Maxwellians.

284 Figure 5 shows the levels of the quasi-thermal plateau in a density-core-temperature
 285 plane with a dipole antenna made of two colinear $L = 2$ m wires, for applications to Parker
 286 Solar Probe/FIELDS. The orange crosses sketch the parameters expected at perihelion
 287 ($n \simeq 7000 \text{ cm}^{-3}$, $T \simeq 10^6 \text{ K}$). We show the power at both the antenna ports, V_f^2 , given by
 288 (36) (left) and at the receiver ports, V_r^2 , (right). The temperature shown on the vertical
 289 axis is T_{-2}^2/T_{-1} , very close to that of the cold Maxwellian when the distribution is a cold
 290 Maxwellian with a suprathermal tail. We have superimposed the approximation (40) as
 291 red bars. In the low frequency range of the plateau, the dipole antenna impedance reduces
 292 to a capacitance [*Meyer-Vernet and Perche, 1989*]

$$C_a \simeq \pi \epsilon_0 L / \ln(L_D/a) \quad (43)$$

293 when $L/L_D \gg 1$, so that one deduces from (7)

$$V_r^2/V_f^2 \simeq 1/(1 + C_b/C_a)^2 \quad (44)$$

294 where C_b is the (dipole) load/stray capacitance, which lumps together the receiver input
 295 capacity and that of the antenna erecting mechanism, including the capacity between
 296 the antenna and the spacecraft structure (the so-called base capacity). With $L = 2$ m,
 297 $a = 1.6 \times 10^{-3}$ m and $L_D \simeq 0.8$ m at 10 solar radii, we have $C_a \simeq 8.9$ pF, whence with
 298 $C_b = 35$ pF (see Table 1), $V_r^2/V_f^2 \simeq 0.04$. This yields a plateau level at the receiver ports
 299 $V_r^2 \simeq 1.7 \times 10^{-15} \text{ V}^2\text{Hz}^{-1}$, which requires a receiver sensitivity of at least a few tens nV
 300 $\text{Hz}^{-1/2}$. These evaluations assume that the ion (Section 2.8) and shot noise contributions

are small enough, which holds in this case, except possibly if the antennas are biased (see Section 3.2).

One sees on Figures 4 and 5 that for smaller values of L/L_D , the plateau level becomes much less sensitive to the temperature; in particular for $L/L_D \simeq 1$, F_0 is nearly proportional to L/L_D , so that the plateau becomes nearly independent of the temperature and cannot be used to measure it; for still smaller lengths, the weak dependence makes the measurement difficult, as is the case for STEREO ($L = 6$ m) at 1 AU.

A very interesting property is that these results also hold in a magnetized plasma if the frequency is a gyroharmonic. Indeed, in that case, as suggested by *Meyer-Vernet et al.* [1993], the magnetic field does not change the QTN level at low frequencies. This can be proven as follows. For $\omega = n\omega_g$, one can factorize in (5) the term $\sum_{-\infty}^{\infty} J_n^2(k_{\perp}v_{\perp}/\omega_g)$ (which is equal to unity [Abramowitz and Stegun, 1965]). Therefore, $\langle \rho^2(\mathbf{k}, n\omega_g) \rangle^{(0)}$ reduces to the value of $\langle \rho^2(\mathbf{k}, 0) \rangle^{(0)}$ in the absence of magnetic field, which is given by (34). Consider now the dielectric function. In a low- β plasma where transverse and longitudinal modes decouple, we can use (2) in the electrostatic limit, and in the expression of the longitudinal permittivity (e.g. [Alexandrov et al., 1984]) one can similarly factorize $\sum_{-\infty}^{\infty} J_n^2(k_{\perp}v_{\perp}/\omega_g) = 1$ when $\omega = n\omega_g$, so that ϵ_L reduces to the low-frequency limit of its unmagnetized value.

This is illustrated in Figure 6, which shows two examples of QTN spectra measured respectively by Wind/Waves in the Earth’s magnetosphere, and by Cassini/RPWS in Saturn’s magnetosphere. One can see that the “plateau” is in these cases the level at the gyroharmonics (except at the lowest frequencies, for which the shot noise and other contributions are not negligible). Note that, since Cassini/RPWS antennas wires are not

324 collinear - making an angle of 120° - with a significant gap between them [*Gurnett et al.*,
325 2004], the antenna response should be changed accordingly [*Schippers et al.*, 2013], using
326 the formulas given in [*Meyer-Vernet and Perche*, 1989].

327 As shown by *Meyer-Vernet et al.* [1993], the frequencies of these minima can be used to
328 measure accurately the modulus of the magnetic field, whereas the increased level between
329 gyroharmonics, produced by the QTN in Bernstein waves (having \mathbf{k} nearly normal to \mathbf{B})
330 - essentially determined by suprathermal electrons [*Sentman et al.*, 1982] - can be used to
331 estimate their energy. The spectra shown in Figure 6 are rather similar to those calculated
332 by *Yoon et al.* [2017] for \mathbf{k} nearly perpendicular to \mathbf{B} (with an integration over k). Note
333 that these calculations are somewhat different from the estimates by *Meyer-Vernet et*
334 *al.* [1993] who include the response of the antenna, so that they find the QTN between
335 gyroharmonics to be roughly proportional to the temperature of hot electrons and to
336 $F_\perp(kL \sin \theta)$ (θ is the angle between the antenna and \mathbf{B} , k corresponds to Bernstein waves
337 and F_\perp is given by (18)-(19)). The factor F_\perp illustrates the interesting counter-intuitive
338 property mentioned in Section 2.2 that a long antenna (with respect to $1/k$) is mainly
339 sensitive to electrostatic waves having \mathbf{k} roughly perpendicular to its proper direction, so
340 that it can receive a large QTN in Bernstein waves when it is oriented relatively close to the
341 magnetic field direction. These calculations have been used to measure the hot electron
342 energy (from the observed power) as well as k (from the modulation with the antenna
343 spin angle) in the Io torus [*Moncuquet et al.*, 1995] and in Saturn's inner magnetosphere
344 [*Moncuquet et al.*, 2005, 2006b].

2.5. Electron Total Density and Kinetic temperature

345 The most basic properties of a particle velocity distribution are the total electron density
 346 and kinetic temperature. In general, these properties are obtained by fitting the QTN
 347 spectrum to the data, except in the ideal case of an antenna much longer than the Debye
 348 length immersed in an isotropic plasma, for which these properties are revealed without
 349 any fitting (Figure 2). Indeed, the QTN spectral peak reveals the plasma frequency -
 350 whence the electron density, and at frequencies $f \gg f_p$ we have $\epsilon_L \simeq 1$, so that (2), (9)
 351 and (33) yield

$$V_f^2 \simeq \frac{32m\omega_p^2}{4\pi\epsilon_0} \int_0^\infty dv v f(v) \int_{\omega/v}^\infty dk F(k)/k^3 \quad \text{for } f \gg f_p \quad (45)$$

352 If $fL/(f_p L_D) \gg 1$, substituting $F(k) \simeq \pi/(4kL)$ in (45) yields

$$V_f^2 \simeq f_p^2 k_B T / (\pi \epsilon_0 L f^3) \quad (46)$$

353 The high-frequency QTN is directly proportional to the kinetic temperature $T \equiv T_2$
 354 whatever the shape of the velocity distribution. This f^{-3} spectrum is clearly seen on
 355 Figure 2. Note that V_f^2 is deduced from the power measured V_r^2 at the receiver ports by
 356 using (44) with the dipole antenna capacitance in this high frequency range

$$C_a \simeq \pi \epsilon_0 L / [\ln(L/a) - 1] \quad (47)$$

357 Such an observation, however, requires that no radioemission perturbs the spectrum. This
 358 can be seen on Figure 7 which shows a radio spectrogram from WIND/WAVES acquired
 359 in the solar wind during the detection of intense solar radioemissions. The power density
 360 below f_p (revealed by the line of increased power), produced by the plasma QTN, remains

361 unperturbed and can still be used to deduce the cold electron temperature (see Section
 362 2.4), but the power is strongly perturbed above f_p and cannot be used for measuring the
 363 kinetic temperature.

364 The total electron density can be deduced from the location of the plasma frequency
 365 peak. However, this peak can be shifted from f_p by several effects. First of all, even in the
 366 absence of Doppler-shifts, the spectral peak may be slightly shifted from f_p , by an amount
 367 which depends on the antenna length (via the factor $F(k)$ in (9) as shown by *Meyer-Vernet*
 368 *and Perche* [1989]), on the distribution of hot electrons and on the frequency and time
 369 resolution, as shown in the following section.

2.6. Hot Electrons

370 Since electrons interact with waves of phase speed equal to their proper speed, and
 371 the phase speed of Langmuir waves $\omega/k \rightarrow \infty$ when $\omega \rightarrow \omega_p$, the shape of the plasma
 372 frequency peak is determined by high speed electrons; the closer the frequency to f_p , the
 373 higher the speed of electrons producing the power. This property is illustrated by the
 374 extreme behaviour of the “square” velocity distribution $f(v) \propto H(v_0 - v)$, the Heaviside
 375 step function, which produces no QTN peak at f_p because of the lack of electrons having
 376 the proper speed to interact with the waves [*Chateau and Meyer-Vernet*, 1989].

377 Detecting very high energy electrons via QTN spectroscopy therefore requires two re-
 378 ceiver properties which may be difficult to conciliate: a high frequency resolution (to
 379 measure accurately the peak shape), and a high temporal resolution (because the space-
 380 craft/plasma relative motion and the turbulence make the electron density near the an-
 381 tenna, whence f_p , change rapidly with time).

382 To illustrate this point, consider an electron velocity distribution made of a sum of
 383 isotropic distributions f_i . From (33), we have

$$\langle \rho^2(\mathbf{k}, \omega) \rangle^{(0)} = \frac{(2\pi e)^2}{k} \sum_i B_i(k) \quad (48)$$

384 where

$$B_i(k) = \int_{\omega/k}^{\infty} dv v f_i(v) \quad (49)$$

385 The imaginary part of the longitudinal dielectric function $\epsilon_L(k, \omega)$ is then

$$\text{Im}(\epsilon_L) = \frac{2\pi^2 e^2 \omega}{\epsilon_0 m k^3} \sum_i f_i(\omega/k) \equiv I_L \quad (50)$$

386 For $\omega/kv \gg 1$, the real part of ϵ_L can be approximated by

$$\text{Re}(\epsilon_L) \simeq 1 - (\omega_p^2/\omega^2) (1 + k^2 \langle v^2 \rangle / \omega^2) \equiv R_L \quad (51)$$

387 whose nearly real zero is

$$k_L \simeq \omega (\omega^2/\omega_p^2 - 1)^{1/2} / (\langle v^2 \rangle)^{1/2} \quad (52)$$

388 The contribution of this zero to the integral (9) (using (2)) can be calculated by writing

389 $R_L \simeq (k - k_L) \partial R_L / \partial k$ for $k \simeq k_L$ at $f \simeq f_p$, with from (51)

$$\partial R_L / \partial k \simeq -2k_L \langle v^2 \rangle / \omega_p^2 \equiv -R'_L \quad (53)$$

390 Therefore (2) and (9) yield for $f = f_p + \Delta f$ with $\Delta f \ll f_p$

$$V_f^2 \simeq \frac{8}{\pi \epsilon_0^2} \frac{F(k_L L)}{k_L^2} \frac{\langle \rho^2(k_L, \omega_p) \rangle^{(0)}}{R'_L(k_L, \omega_p) I_L(k_L, \omega_p)} \quad (54)$$

391 Substituting (48), (50) and (53) yields the shape of the QTN peak

$$V_f^2 \simeq \frac{8m v_{ph} F(\omega_p L / v_{ph})}{\pi \epsilon_0 \langle v^2 \rangle} \left[\frac{\sum_i \int_{v_{ph}}^{\infty} dv v f_i(v)}{\sum_i f_i(v_{ph})} \right] \quad (55)$$

392 where

$$v_{ph} \simeq \omega_p / k_L \simeq (\langle v^2 \rangle f_p / 2 \Delta f)^{1/2} \simeq [(3k_B T / 2m)(f_p / \Delta f)]^{1/2} \quad (56)$$

393 and in (55)-(56), $\langle v^2 \rangle$ and T (the kinetic temperature) concern the whole velocity dis-
 394 tribution. One sees from (55) that the noise at frequency $f = f_p + \Delta f$ is produced by
 395 electrons moving faster than v_{ph} given by (56). The detailed shape of the peak is governed
 396 by the value of $\omega_p L / v_{ph}$ (determining F given by (10)) and by the electron population f_i
 397 that dominates the bracket in (55). If $f(v) \simeq f_i(v)$ for $v \geq v_{ph}$, the same population i
 398 dominates both the numerator and the denominator of this bracket, which simplifies to

$$[\dots] \simeq \int_{v_{ph}}^{\infty} dv v f_i(v) / f_i(v_{ph}) \quad (57)$$

399 Hence in that case the amplitude and shape of the QTN peak depend only on the shape
 400 of the component i of the distribution and not of its relative density.

401 Consider the case when at speeds $v \gtrsim v_{ph}$, the distribution can be approximated by a hot
 402 Kappa halo given by (27) with density n_h and temperature $T_h = (m v_0^2 / 2k_B)[\kappa / (\kappa - 3/2)]$.
 403 With for example $n_h / n = 0.05$, $T_h / T = 10$ and $\kappa = 5$, one can verify that this holds when
 404 $\Delta f / f_p \lesssim 0.1$ (when the core is Maxwellian). The bracket in (55) then reduces to

$$[\dots] \simeq \frac{k_B T_h \kappa - 3/2}{m \kappa} \left[1 + \frac{3T}{4T_h(\kappa - 3/2)} \frac{f_p}{\Delta f} \right] \quad (58)$$

405 When $\Delta f/f_p > 3T/[4T_h(\kappa - 3/2)]$, which holds with the above parameters when $\Delta f/f_p >$
 406 0.02, the bracket in (58) reduces to unity in order of magnitude, so that (55) and (58)
 407 yield

$$V_f^2 \simeq \frac{8mv_{ph}F(\omega_p L/v_{ph})}{3\pi\epsilon_0} \frac{T_h \kappa - 3/2}{T \kappa} \quad (59)$$

408 An interesting property emerges from (59). In this exterior part of the peak ($0.02 <$
 409 $\Delta f/f_p < 0.1$ with the above parameters), the power is not only independent of the
 410 density of the halo, it is also similar for a Kappa halo and a Maxwellian halo ($\kappa \rightarrow \infty$),
 411 if they have similar most probable speeds ($v_0 = [(\kappa - 3/2) \times T_h/\kappa]^{1/2}$, from (28)). Let us
 412 estimate the amplitude of the peak in this frequency range. We have from (56) and (26)

$$\frac{\omega_p L}{v_{ph}} \simeq \frac{L}{L_D} \left(\frac{T_{-2}}{T} \right)^{1/2} \left(\frac{2\Delta f}{3f_p} \right)^{1/2} \quad (60)$$

413 For $\Delta f/f_p \simeq 0.05$ (which lies in the range determined above) and $L/L_D < 5$, (60) yields
 414 $\omega_p L/v_{ph} < 1$, so that $F(\omega_p L/v_{ph}) \simeq (\omega_p L/v_{ph})^2/24$ and (59) and (56) yield $V_f^2/T^{1/2} \simeq$
 415 5×10^{-16} for $L/L_D \simeq 5$.

416 Closer to f_p ($\Delta f/f_p < 0.02$ in our example), the right-hand side term of the bracket in
 417 (58) becomes dominant, which means that v_{ph} is such that the electrons producing the
 418 noise are in the speed range where the hot kappa distribution (27) behaves as a power
 419 law velocity distribution $f(v) \propto v^{-p}$ with $p = 2(\kappa + 1)$. In that case, (58) yields

$$[\dots] \simeq \frac{3k_B T}{4m\kappa} \frac{f_p}{\Delta f} \quad (61)$$

420 which no longer depends on T_h (nor n_h), and we get from (55), (56), (11), (60) and (61)

$$V_f^2 \simeq \frac{(mk_B T)^{1/2} T_{-2} L^2}{6^{3/2} \pi \epsilon_0 \kappa T L_D^2} \left(\frac{f_p}{\Delta f} \right)^{1/2} \quad (62)$$

421 so that the power increases strongly very close to f_p , as $(f_p/\Delta f)^{1/2}$, yielding a peak located
 422 at f_p . This contrasts with the behavior for a Maxwellian halo ($\kappa \rightarrow \infty$), in which case
 423 the bracket (58) equals $k_B T_h/m$, so that (55) yields

$$V_f^2 \simeq \frac{8mT_h v_{ph}}{3\pi\epsilon_0 T} F(\omega_p L/v_{ph}) \quad (63)$$

424 Equation (63) shows that when $\Delta f \rightarrow 0$ ($v_{ph} \rightarrow \infty$), $V_f^2 \rightarrow 0$, so that the noise peak
 425 is shifted above f_p [Meyer-Vernet and Perche, 1989], at the value of Δf for which
 426 $v_{ph} F(\omega_p L/v_{ph})$ is maximum.

427 Let us use these results to determine whether QTN spectroscopy can be used to measure
 428 the solar wind super-halo electrons, which have a nearly isotropic power-law velocity
 429 distribution at energies exceeding $E_0 \simeq 2$ keV [e.g., Wang *et al.*, 2012]. Using v_{ph} given
 430 by (56), we see that these electrons are revealed at frequencies $f_p + \Delta f$ with $\Delta f/f_p <$
 431 $(3/4) \times T_{eV}/E_0 \simeq 4 \times 10^{-3}$ if $T \simeq 10$ eV. Such an observation also requires that the f_p
 432 fluctuations produced by turbulent density fluctuations [e.g., Wang *et al.*, 2012] occurring
 433 during the measurement of the peak do not broaden it by more than Δf , which imposes
 434 a constraint on the time resolution that may be difficult to conciliate with the frequency
 435 resolution (because of the Nyquist-Shannon theorem). Using (62) with $\kappa = p/2 - 1$, we
 436 obtain for $p = 7$ and $L/L_D = 5$, $V_f^2/T^{1/2} \simeq 10^{-16} (f_p/\Delta f)^{1/2}$. For $\Delta f/f_p \simeq 4 \times 10^{-3}$,
 437 this yields $V_f^2/T^{1/2} \simeq 1.4 \times 10^{-15} \text{ V}^2\text{Hz}^{-1}$, i.e. about $4 \times 10^{-13} \text{ V}^2\text{Hz}^{-1}$ for $T \simeq 10^5$

438 K. Since $(1/\Delta f) \int_{f_p}^{f_p+\Delta f} df [f_p/(f - f_p)]^{1/2} = 2$, a receiver with this frequency resolution
 439 should measure twice this power, i.e. $V_f^2 \simeq 10^{-12} \text{ V}^2\text{Hz}^{-1}$.

440 It is interesting to note that such a very high noise level, corresponding to QTN pro-
 441 duced by super-halo electrons, could be erroneously interpreted instead as due to plasma
 442 instabilities.

2.7. Flat-top Distributions

443 Flat-top distributions are observed in various media, under conditions when all particles
 444 are accelerated up to a similar energy, for example via an electrostatic field present in a
 445 restricted region. Such velocity distributions have been observed in particular in the
 446 Earth’s magnetosheath [*Feldman et al.*, 1982], the Earth’s magnetotail around magnetic
 447 reconnection regions [*Asano et al.*, 2008], and downstream of strong interplanetary shocks
 448 [*Fitzenreiter et al.*, 2003].

449 Compared to Maxwellians or Kappas, for which the bulk of the distribution has a rela-
 450 tively similar shape, flat-top distributions have a large excess of medium energy particles,
 451 and the “temperatures” defined in (20)-(22) with $q < 0$ generally exceed the kinetic
 452 temperature T_2 , contrary to distributions with suprathermal tails. For example, the dis-
 453 tribution studied by *Chateau and Meyer-Vernet* [1989], $f(v) \propto [1 + (v/v_0)^8]^{-1}$, which can
 454 approximate distributions measured in the Earth’s magnetosheath, has $T_{-2} = 1.24 \times T$
 455 with $T \equiv T_2 = mv_0^2/3k_B$, so that the Debye length largely exceeds that of a Maxwellian of
 456 similar temperature. Since in this case $T_{-1} = 1.11 \times T$, we have $T_{-2}/T_{-1}^{1/2} = 0.95 \times T_{-2}^{1/2}$,
 457 so that the temperature deduced from the plateau level using (40) is close to that defining
 458 the Debye length. However, since $T_{-2}^2/T_{-1} = 1.37 \times T$ this “temperature” exceeds by
 459 nearly 40% the kinetic temperature T revealed by the high-frequency QTN using (46) - a

460 behavior which strongly contrasts with that of a Kappa distribution. Therefore, although
 461 the QTN diagnostics cannot reveal the full flat-top shape, it can nevertheless give a strong
 462 hint of such a shape.

2.8. Ions

463 Because of their large mass (small characteristic frequency), ions generally play a minor
 464 role in the QTN at frequencies of the order of magnitude of the plasma frequency, except
 465 when the Doppler-shift of their fluctuations puts them in this frequency range - a case often
 466 encountered in the solar wind. Since Ulysses spin axis was close to the solar direction, the
 467 equatorial antennas were oriented approximately perpendicular to the solar wind velocity.
 468 The contribution of the solar wind ions to the QTN has been calculated in this case
 469 [Issautier *et al.*, 1999] and used to estimate the ions properties [Issautier *et al.*, 1998]. We
 470 derive below a few additional properties that may be useful for other missions.

471 Equations (2), (3) and (13) show that if the drift speed is much larger than the ion
 472 average speed, the main contribution to the integral in (13) stems from the values of θ
 473 satisfying $\omega \simeq kV \cos \theta$. Hence if the antenna is parallel to the drift speed we deduce
 474 by substituting $k \cos \theta = \omega/V$ into (16) that the ion QTN is proportional to the factor
 475 $[\sin^2(\omega L/2V)/(\omega L/V)]^2$, which oscillates with frequency and goes to zero at frequencies
 476 that are multiples of V/L . Such variations have been observed on WIND/WAVES [Tong
 477 *et al.*, 2015].

478 An important simplification arises when $\omega L_D/V \gg 1$, which holds around the plasma
 479 frequency in the solar wind for PSP at 10 solar radii ($\omega_p L_D/V \simeq 20$). In that case, the

480 QTN contribution due to the ions is given by

$$V_{\text{fions}}^2 \simeq \frac{8m_e V^3 \omega_p^2}{\pi \epsilon_0 L^2 \omega^4} \sin^4\left(\frac{\omega L}{2V}\right) \quad \text{antenna} \parallel \mathbf{V} \quad (64)$$

$$V_{\text{fions}}^2 \simeq \frac{m_e V^2 \omega_p^2}{\epsilon_0 L \omega^3} \quad \text{antenna} \perp \mathbf{V} \quad (65)$$

481 Comparing with (41), one sees that the ion contribution to the QTN is expected to be
 482 negligible whatever the antenna direction for PSP at perihelion.

3. QTN in Real Life

483 Now that QTN spectroscopy has been admitted in the exclusive club of recognized in
 484 situ measurement techniques, it is essential to ensure that it is not used loosey-goosey,
 485 under conditions which might lead to incorrect results. We therefore discuss below some
 486 constraints of real life in space which are (or are not) compatible with accurate measure-
 487 ments by QTN spectroscopy, and derive some results that may be useful for practical
 488 applications.

3.1. Unequal Booms

489 When the antenna wires are too thin, they can be broken by dust impacts. This
 490 happened several times for the WIND/WAVES dipole antennas, which now have arms of
 491 unequal length. We consider below an antenna made of two wires of respective lengths
 492 L_1 and L_2 , aligned along the z axis and longer than the gap between them (we do not
 493 consider the effect of a gap since this has been calculated by *Meyer-Vernet and Perche*
 494 [1989]).

495 The Fourier transform of the current distribution becomes

$$J_z(\mathbf{k}) = \frac{1}{k_z^2} \left[\frac{e^{ik_z L_1} - 1}{L_1} + \frac{e^{-ik_z L_2} - 1}{L_2} \right] \quad (66)$$

496 Hence with an isotropic velocity distribution, the QTN is obtained by replacing in (9)

497 $F(kL)$ by $G(kL_1, kL_2)$ given by

$$G(kL_1, kL_2) = \frac{1}{4k} \left(\frac{L_1 + L_2}{L_1 L_2} \right) \{g(kL_1) + g(kL_2) - g[k(L_1 + L_2)]\} \quad (67)$$

$$g(x) = \frac{\cos x - 1}{x} + \text{Si}(x) \quad (68)$$

498 where Si is the sine integral function. In the particular cases of respectively short and

499 long antennas, (67)-(68) yield

$$G(kL_1, kL_2) \simeq \frac{k^2(L_1 + L_2)^2}{96} \quad \text{if} \quad kL_1, kL_2 \ll 1 \quad (69)$$

$$G(kL_1, kL_2) \simeq \frac{\pi}{8k} \frac{L_1 + L_2}{L_1 L_2} \quad \text{if} \quad kL_1, kL_2 \gg 1 \quad (70)$$

500 Therefore for short antennas, the unequal arms of lengths L_1, L_2 are equivalent to a

501 symmetric antenna made of wires of length the average length, $L_a = (L_1 + L_2)/2$, whereas

502 for long antennas, the unequal arms are equivalent to an antenna of length the inverse of

503 the average of the inverse lengths, $L_g = 2L_1 L_2 / (L_1 + L_2)$. In the frequent case when the

504 antenna is short compared to the electromagnetic wavelength c/f , but long with respect

505 to L_D , this property suggests a quick method for determining separately the lengths of

506 the two antenna arms when they have been broken, using both a known radioemission as

507 the galactic noise and the QTN in a known plasma. Indeed in that case, (69) shows that

508 the reception of electromagnetic waves depends on the arithmetic mean L_a , whereas (70)

509 shows that the QTN depends on the geometric mean L_g ; this enables one to determine

510 both L_g and L_a , from which one can deduce directly L_1 and L_2 . When the booms are not

511 long enough to use the approximation (70), one must use the exact expression (67).

3.2. Fat and/or Biased Antennas

512 To be adequate for thermal noise spectroscopy, electric antennas must not only be long
 513 enough (albeit not too long [*Meyer-Vernet et al.*, 2000]), they must also be thin enough.
 514 There are two basic constraints on the radius of electric antennas. First its must be small
 515 compared to the Debye length, otherwise the approximation $k_{\perp}a \ll 1$ in Eq.(8) does
 516 not hold true, producing additional resonances - a problem only encountered in dense
 517 planetary ionospheres; a further problem arises in that case (see Section 4). The second
 518 constraint is due to the shot noise, since fat antennas may collect or emit so many electrons
 519 that the corresponding shot noise may exceed the quasi-thermal noise. Since each electron
 520 collection or emission from or to the ambient plasma produces a voltage pulse of rise time
 521 $\sim (2\pi f_p)^{-1}$ ($\sim (2\pi f_{ph})^{-1}$ for photoelectrons of plasma frequency f_{ph}) and a generally
 522 much longer decay time, τ_d , due to the discharge of the antenna, the shot noise has a f^{-2}
 523 spectrum for $(2\pi\tau_d)^{-1} < f < f_p$ (the squared Fourier transform of a Heaviside function).
 524 In practice, if the electron collection is not much affected by the antenna electric potential
 525 Φ (which requires the condition $e|\Phi| \ll k_B T_e$), the shot noise below the plasma frequency
 526 at the antenna ports can be approximated by

$$V_{\text{shot}}^2 \simeq 2|I_{e0}| \times e/C_a^2 \omega^2 \simeq 2 \times 10^{-16} (a/L) [\ln(L_D/a)]^2 T_1^{1/2} (f_p/f)^2 \quad (71)$$

527 for $a < L_D < L$ (from Eq.(25) and the formulas by [*Meyer-Vernet and Perche*, 1989]),
 528 where $C_a \simeq (i\omega Z_a)^{-1}$ is the dipole antenna capacitance and I_{e0} is the electron current
 529 on one antenna arm when $\Phi = 0$. Comparing with the expression (40) of the QTN, (71)
 530 yields

$$V_{\text{shot}}^2/V_{\text{QTN}}^2 \simeq 4.9 \times \tau(a/L)[\ln(L_D/a)]^2(f_p/f)^2 \quad (72)$$

531 with $\tau = T_1^{1/2}T_{-1}^{1/2}/T_{-2}$, which equals unity for a Maxwellian electron distribution, whereas
 532 $\tau \gtrsim 1$ when the distribution has a suprathermal tail; for example, with a Kappa distri-
 533 bution we have $\tau = (\kappa - 1/2)/(\kappa - 1)$. With the parameters listed in Table 1 and $\tau \simeq 1$,
 534 (72) yields $V_{\text{shot}}^2/V_{\text{QTN}}^2 \simeq 0.4 \times (f_p/f)^2$ for SO and $V_{\text{shot}}^2/V_{\text{QTN}}^2 \simeq 0.14 \times (f_p/f)^2$ for PSP
 535 at perihelion. As noted above, these results assume the frequency to be smaller than f_p
 536 and to exceed the inverse of the decay time $\tau_d \simeq RC_a$ of the antenna potential pulses pro-
 537 duced by electron impacts and emission, so that these pulses are roughly step-like; here
 538 R is the low-frequency antenna resistance due to its discharge by photoelectron emission
 539 and plasma collection [*Henri et al.*, 2011]; at smaller frequencies the shot noise is smaller
 540 by the factor $\omega\tau_d$.

541 The expression (71) of the shot noise also assumes both that the electron collection
 542 is not much affected by the antenna electric potential Φ , and that this potential is the
 543 floating potential for which the electron collection current is mainly balanced by the
 544 photoelectron emission current or by the ion current if the latter is larger. This may not
 545 be the case if the antenna is biased since in that case the change in antenna potential
 546 may change significantly the number of elementary charges transferred from and to the
 547 antennas, whereas the bias current, I_b , also contributes to the shot noise. Indeed, since
 548 each individual charge transfer to the antenna contributes additively to the shot noise,
 549 positive and negative current pulses do not cancel out and they all contribute to the
 550 fluctuations.

551 Let us first consider the case when the ambient medium is the solar wind. In this case,
 552 the photoelectron current I_{ph0} typically exceeds the plasma electron current I_{e0} by one
 553 order of magnitude (here the subscript '0' stands for the currents on an antenna arm
 554 when $\Phi = 0$). Hence the antenna potential Φ floats at a few times the photoelectron
 555 temperature $T_{ph(eV)}$, in order that the ejected photoelectron current

$$I_{ph} \simeq I_{ph0} \times e^{-\Phi/T_{ph(eV)}} \quad (73)$$

balances the collected electron current

$$I_e \simeq I_{e0} \times (1 + \Phi/T_{e(eV)}) \quad (74)$$

556 where we have assumed Maxwellian distributions with $\Phi/T_{e(eV)} \ll 1$ since $T_{ph} \ll T_e$
 557 [Whipple, 1981]. In that case, the shot noise (71) is increased by the factor $I_e/I_{e0} \simeq$
 558 $(1 + \Phi/T_{e(eV)})$. This result also holds in presence of secondary electron emission I_{sec} since
 559 in that case $|I_{sec}| + |I_{ph}| = |I_e|$ (neglecting the smaller ion current). Note that we have
 560 neglected the shot noise produced by the photoelectrons returning to the antenna because
 561 at frequencies $f < f_p$ the corresponding pulse duration ($\simeq 1/(2\pi f_{ph})$) is much shorter than
 562 $1/(2\pi f)$.

563 If the antenna is biased with a bias current I_b (per antenna arm), the shot noise (71)
 564 becomes

$$V_{\text{shot}}^2 \simeq (|I_e| + |I_{ph}| + |I_b|)e/C_a^2\omega^2 \quad (75)$$

565 since it is proportional to the total number of elementary charges transferred from or to
 566 the antenna per time unit, and the contribution of the bias current to the shot noise is

567 estimated by assuming that the corresponding impedance is essentially due to the antenna
 568 capacitance. Since $I_b = |I_{ph}| - |I_e|$, we deduce

$$V_{\text{shot}}^2 \simeq 2e \times \text{Max}(|I_{ph}|, |I_e|) / C_a^2 \omega^2 \quad (76)$$

569 Consider the case when, due to the bias, the antenna potential becomes much smaller
 570 than both $T_{ph(\text{eV})}$ and $T_{e(\text{eV})}$, so that $|I_{ph}| \simeq |I_{ph0}|$ and $|I_e| \simeq |I_{e0}| \ll |I_{ph}|$. In that case
 571 (76) shows that the bias increases the shot noise (71) by the approximate factor $|I_{ph0}/I_{e0}|$,
 572 which amounts to about one order of magnitude in the solar wind; such a bias would make
 573 the shot noise largely dominant over the QTN for SO and of the same order of magnitude
 574 as the QTN for PSP. On the other hand, biasing the antenna in order to increase its
 575 positive potential Φ would increase the shot noise by a smaller factor. Note that the
 576 above estimates assume the antenna photoelectron current to be given by (73), even at
 577 small heliocentric distances because - contrary to the spacecraft PSP [Ergun *et al.*, 2010]
 578 - the antennas, whose radius is smaller than the photoelectron Debye length, are not
 579 expected to be surrounded by a potential barrier reflecting the emitted photoelectrons.

580 Consider now dense planetary environments, when the plasma ion current dominates the
 581 photoelectron current. In that case, since $|I_{i0}/I_{e0}| \simeq (m_e T_{1i}/m_i T_{1e})^{1/2} \ll 1$, the antenna
 582 potential floats to a negative value of order a few times the plasma electron temperature in
 583 order to decrease the plasma electron current $I_e \simeq I_{e0} \times e^{-|\Phi|/T_{e(\text{eV})}}$ sufficiently to balance
 584 the plasma ion current given by $I_i \simeq I_{i0} \times (1 + |\Phi|/T_{i(\text{eV})})$ for $\Phi/T_{i(\text{eV})} \ll 1$ [Whipple,
 585 1981]. In that case, the shot noise (71) is decreased by the factor $I_e/I_{e0} \simeq e^{-|\Phi|/T_{e(\text{eV})}}$.

586 With a bias current, the shot noise is given by (75)-(76) with $|I_{ph}|$ replaced by $|I_i|$. In
 587 that case, if because of the bias, the potential $|\Phi|$ becomes much smaller than both $T_{i(\text{eV})}$

588 and $T_{e(\text{eV})}$, we have $|I_i| \simeq |I_{i0}|$ and $|I_e| \simeq |I_{e0}| \gg |I_i|$, so that $\text{Max}(|I_i|, |I_e|) \simeq |I_{e0}|$ and the
 589 shot noise is thus given by (71). In contrast, a bias making the antenna potential more
 590 negative would decrease the shot noise.

3.3. Dusty Plasmas: Quasi-Thermal Noise of Charged Dust Grains

591 Virtually every plasma contains dust particles [*Shukla and Mamun*, 2002]. They can af-
 592 fect plasma waves in two ways. First, when dust grains impact solid surfaces at high-speed,
 593 they are vaporized and partially ionized, as well as the material of the impacted surface;
 594 this produces an expanding plasma cloud which affects the ambient electric field, whereas
 595 some plasma particles are recollected by the spacecraft or antennas; these processes can be
 596 detected by radio receivers and are currently used for dust detection (e.g. *Meyer-Vernet*
 597 *et al.* [2016] and references therein) complementary to dedicated dust detectors (e.g. *Auer*
 598 [2001]). Second, since dust grains carry electric charges (e.g. *Mann et al.* [2014]), their
 599 motion produces an electric field, which can be detected by the electric antennas. We
 600 consider below the latter mechanism, and assume that the concentration of dust grains is
 601 small enough that they do not affect the plasma dielectric function [*Verheest*, 1996].

In order to compare this mechanism to impact ionization, consider the charge carried
 by a dust particle of radius r_d and floating potential Φ_d

$$q \simeq 4\pi\epsilon_0 r_d \Phi_d \quad (77)$$

602 where Φ_d equals a few times the temperature (in eV) of the particles that govern the grains'
 603 charging, i.e., photoelectrons in the solar wind or ambient electrons in dense planetary
 604 environments. Beware that (77) no longer holds when the grain's size is smaller than
 605 the Landau radius (the distance at which the mutual electrostatic energy of two plasma

606 electrons equals their thermal energy), because of both the grains' polarization and the
 607 charge quantization [e.g., *Meyer-Vernet*, 2013].

608 Comparing q with the charge involved in impact ionization for a grain of mass m_d
 609 impacting at speed v_d , $Q \simeq 0.7m_d v_{d(\text{km/s})}^{3.5}$ [*McBride and McDonnell*, 1999; *Lai et al.*,
 610 2002], we have

$$q/Q \simeq 0.015 \times r_{d(\mu\text{m})}^{-2} v_{d(\text{km/s})}^{-3.5} \Phi_d \quad (78)$$

611 Equation (78) generally yields $q/Q \ll 1$, except for submicron particles moving slowly, for
 612 example nanodust that have not yet been accelerated, such as freshly produced nanodust
 613 in the solar wind or nanodust in inner planetary magnetospheres.

614 Let us now compare the number of dust particles affecting the electric antennas in
 615 dipole mode for both mechanisms. The rate of passing-by dust particles affecting the
 616 antennas exceeds the impact rate on their surface by the large factor L_D/a , of order of
 617 magnitude 10^4 for the cases listed in Table 1 (we do not consider the impacts on the
 618 spacecraft, which are generally not efficiently detected in dipole mode). These numbers
 619 suggest that the electric noise produced by dust grains passing by the antennas may be
 620 worth considering. Such a measurement via a time domain sampler has been discussed
 621 by *Meuris et al.* [1996]. We consider below the possibility of such a measurement via a
 622 wave receiver, i.e. the quasi-thermal noise produced by dust grains moving around the
 623 antennas.

624 In order to derive order-of-magnitude estimates, we consider a simple case: dust grains
 625 of charge q and isotropic velocity distribution $f_d(v)$. From Eqs. (2), (9) and (33), their
 626 QTN is given by

$$V_{fd}^2 = \frac{32q^2}{\epsilon_0^2} \int_0^\infty dk \frac{F(kL)}{k^3 |\epsilon_L(\mathbf{k}, \omega)|^2} \int_{\omega/k}^\infty dv v f_d(v) \quad (79)$$

627 where $F(x)$ is given by (10). We now make the further simplifying assumption that the
628 grains have a similar speed V_d , so that their distribution can be approximated by

$$f_d(v) = n_d \delta(v - V_d) / (4\pi V_d^2) \quad (80)$$

629 n_d being their number density. Substituting (80) into (79) yields

$$V_{fd}^2 = \frac{8n_d q^2}{\pi \epsilon_0^2 V_d} \int_{\omega/V_d}^\infty dk \frac{F(kL)}{k^3 |\epsilon_L(\mathbf{k}, \omega)|^2} \quad (81)$$

630 Since V_d is much smaller than the electron thermal speed, we can use the approximation
631 (35) of ϵ_L in the integral (81), which reduces to $\epsilon_L \simeq 1$ since $kL_D \gg 1$ in the integration
632 range. This yields the QTN of this dust distribution

$$V_{fd}^2 = \frac{8n_d q^2 L^2}{\pi \epsilon_0^2 V_d} \int_{\omega L/V_d}^\infty dx \frac{F(x)}{x^3} \quad (82)$$

633 Using the approximations (11) and (12), we deduce in particular

$$V_{fd}^2 = \frac{2n_d q^2 V_d^2}{3\epsilon_0^2 L \omega^3} \quad \text{for } \omega L/V_d \gg 1 \quad (83)$$

$$V_{fd}^2 = \frac{n_d q^2 L^2}{3\pi \epsilon_0^2 V_d} \ln(V_d/\omega L) \quad \text{for } \omega L/V_d \ll 1 \quad (84)$$

634 For example, a concentration $n_d \simeq 10^3 \text{ cm}^{-3}$ of nanodust of radius a few nanometers
635 moving at $V_d \simeq 15 \text{ km/s}$ relative to the Cassini spacecraft in Enceladus' plume [*Hill et*
636 *al.*, 2012] should produce from (83) a QTN power of order of magnitude $V_{fd}^2 \simeq 10^{-10}$
637 V^2Hz^{-1} near 1 kHz. This level is expected to largely exceed the shot noise due to plasma
638 particle impacts because of the strong electron depletion [*Hill et al.*, 2012].

4. Concluding Remarks

639 We have provided a number of new tools for implementing QTN spectroscopy in space
640 plasmas, which are generally not in thermal equilibrium and are sometimes dusty, inboard
641 various missions. In particular, we give an exact generic expression of the “cold” electron
642 temperature and of its measurement via the QTN plateau (36); we also give a generic
643 analytical approximation (40) of this plateau valid for practical antenna lengths in space,
644 and provide an application for PSP at perihelion. The QTN plateau level is all the
645 more generic, given that we have proven that it still holds in presence of a magnetic
646 field. We also give new analytical approximations of the QTN peak shape and level in
647 several practical cases, and study the conditions in which the solar wind super halo might
648 be measured by this technique. Concerning flat-top distributions, we suggest a simple
649 method to infer them by comparing the low and high frequency QTN levels. Finally, we
650 give new analytical approximations for the QTN due to ions in the solar wind, and show
651 that this component is expected to be negligible for PSP at perihelion.

652 In order to adapt the method to various practical situations in space, we have considered
653 antennas made of two wires of different lengths, as occurs on WIND after damaging of
654 the antennas by dust impacts, and suggest a new method for determining separately the
655 lengths of the dipole arms. We also consider fat and/or biased antennas, showing that
656 biasing might considerably increase the shot noise in the solar wind, possibly spoiling
657 QTN measurements. Finally, we have estimated the QTN produced by the motion of
658 dust grains near the antennas, yielding a new method to measure grains when their speed
659 is not high enough for producing significant impact ionization. This result may be applied
660 for detecting nanodust in the Enceladus plume, where the plasma shot noise is expected to

661 be small because of the strong electron depletion (due to capture of most plasma electrons
662 by the grains) [*Hill et al.*, 2012], so that the dust QTN noise may dominate the spectrum
663 at low frequencies.

664 Further extensions will be necessary in the near future to implement QTN spectroscopy
665 on the cubesat projects [e.g., *Swartwout*, 2013; *Saint-Hilaire et al.*, 2014] in the Earth's
666 ionosphere. Even though collisions are negligible at normal cubesat altitudes, they should
667 be taken into account at lower altitudes (the E region); such an extension has already been
668 considered [*Meyer and Vernet*, 1975; *Martinovic et al.*, 2017]. Another simple extension
669 which has already been considered [*Meyer-Vernet and Perche*, 1989] is the accounting of
670 the gap between antenna arms due to the presence of the satellite if its diameter is not
671 small compared to the antenna length. A much more difficult problem is that the negative
672 floating potential of the antenna, of modulus greater than the electron temperature (in
673 eV) will produce a sheath depleted of electrons around the antenna, of width several Debye
674 lengths [*Laframboise*, 1966], because the antenna radius will not be small compared to
675 the Debye length (typically a fraction of centimeter). A detailed study of the impedance
676 of a wire dipole antenna in the Earth's ionosphere has shown that this effect can be
677 approximately taken into account at frequencies $f > f_p$ by making a simple extension of
678 the theory [*Meyer and Vernet*, 1975], putting in series the impedance of an antenna of
679 radius comparable to that of the sheath, G (the antenna radius plus a few Debye lengths)
680 and that corresponding to the capacitance of a vacuum sheath ($\pi\epsilon_0 L / \ln(G/a)$). However,
681 at frequencies $f < f_p$, a new effect arises: the local plasma frequency in some region of the
682 depleted sheath equals the frequency f , yielding resonances with associated non-collisional
683 losses [*Meyer-Vernet et al.*, 1977]. This effect produces a strong increase of the antenna

684 resistance [*Meyer-Vernet et al.*, 1978] (and therefore of the QTN) and requires a major
685 extension of the theory to be accounted for.

686 Other extensions will be necessary for applications in the inner solar system. The elec-
687 tron distribution close to the Sun is expected to have significant anisotropies, in particular
688 due to the suprathermal electrons focused along the magnetic field - the so-called strahl
689 [e.g., *Marsch*, 2006]. The effects of electron temperature anisotropies on the QTN at low
690 and high frequencies have been estimated by *Meyer-Vernet* [1994], whereas the effects of
691 the electron bulk speed on the QTN cut-off at the plasma frequency have been considered
692 by *Issautier et al.* [1999]. However, the effects of drift or focusing of suprathermal elec-
693 trons, which is an important topic, has not yet been studied. And since Nature always
694 turns out to be subtler than we imagine, the future diagnostics will most probably require
695 further and as yet unanticipated extensions of the QTN theory.

696
697 **Acknowledgments.** The authors thank the CNES and the CNRS for support on the
698 Ulysses/URAP, Wind/WAVES and Cassini/RPWS HF projects, and Mélody Pallu and
699 Mathieu Vachey for their help on data processing for Figure 6. The data presented in this
700 paper can be accessed by contacting the authors.

References

- 701 Abramowitz, M. and I. A. Stegun (1965), *Handbook of mathematical functions*, Dover,
702 New York.
- 703 Alexandrov, A. F., L. S. Bogdankevich and A. A. Rukhadze (1984), *Principles of plasma*
704 *electrodynamics*, Springer, Berlin, p. 114.

- 705 Asano, Y. et al. (2008) Electron flat-top distributions around the magnetic reconnection
706 region, *J. Geophys. Res.*, *113*, A01207, DOI: 10.1029/2007JA012461.
- 707 Auer, S. (2001) Instrumentation, in *Interplanetary Dust*, ed. E. Grün, B. A. S. Gustafson,
708 S. Dermott and H. Fechtig (Heidelberg:Springer), 385-444.
- 709 Bale, S. D. et al. (2016), The FIELDS instrument suite for Solar Probe Plus, *Space Sci.*
710 *Rev.*, DOI: 10.1007/s11214-016-0244-5.
- 711 Chateau, Y. F., N. Meyer-Vernet (1989) Electrostatic Noise in Non-Maxwellian Plasmas:
712 “Flat-Top” Distribution Function, *J. Geophys. Res.*, *94*, 15,407-15,414.
- 713 Chateau, Y. F., N. Meyer-Vernet (1991) Electrostatic noise in non-Maxwellian plasmas:
714 Generic properties and “kappa” distributions, *J. Geophys. Res.*, *96*, 5825-5836.
- 715 Couturier, P., S. Hoang, N. Meyer-Vernet and J.-L. Steinberg (1981) Quasi-thermal noise
716 in a stable plasma at rest: theory and observations from ISEE 3, *J. Geophys. Res.*, *86*,
717 11,127-11,138.
- 718 Dudík et al. (2017), Non-equilibrium processes in the solar corona, transition region, flares,
719 and solar wind, *Solar Physics*, *xx*, xx.
- 720 Ergun, R. E. et al. (2010), Spacecraft charging and ion wake formation in the near-Sun
721 environment, *Phys. of Plasmas*, *17*, 072903, doi:10.1063/1.3457484.
- 722 Fahr, H. J., M. Heyl (2016) Debye screening under non-equilibrium plasma conditions,
723 *Astron. Astrophys.*, *589*, A85.
- 724 Fejer, J. A., J. R. Kan (1969) Noise spectrum received by an antenna in a plasma, *Radio*
725 *Sci.*, *4*, 721-728.
- 726 Feldman, W. C. et al. (1982) Electron heating within the Earth’s bow shock, *Phys. Rev.*
727 *Lett.*, *49*, 199.

- 728 Fitzenreiter, R. J., Ogilvie, K., W., Bale, S. D., Vinãs, A. F. (2003) Modification of the
729 solar wind electron velocity distribution at interplanetary shocks, *J. Geophys. Res.*, *108*,
730 1415-1979, DOI: 10.1029/2003JA009865.
- 731 Garrett, H. B. (1981), The charging of spacecraft surfaces, *Rev. Geophys. Space Phys.*,
732 *19*, 577-616.
- 733 Gurnett, D. A. et al. (2004), The Cassini radio and plasma wave investigation, *Space Sci.*
734 *Rev.*, *114*, 395-463.
- 735 Henri, P. et al. (2011), Observations of Langmuir ponderomotive effects using the Solar
736 TERrestrial RELations Observatory spacecraft as a density probe, *Physics of Plasmas*,
737 *18*, 082308.
- 738 Hill, T. W. et al. (2012), Charged nanograins in the Enceladus plume, *J. Geophys. Res.*,
739 *117*, A05209.
- 740 Hoang, S., J.-L. Steinberg, G. Epstein, P. Tilloles, J. Fainberg, R. G. Stone (1980), The
741 low-frequency continuum as observed in the solar wind from ISEE 3 - Thermal electro-
742 static noise, *J. Geophys. Res.*, *85*, 3419-3430.
- 743 Hoang, S. et al. (1992), Solar wind thermal electrons in the ecliptic plane between 1 and
744 4 AU - Preliminary results from the ULYSSES radio receiver, *Geophys. Res. Lett.*, *19*,
745 1295-1298.
- 746 Issautier, K., N. Meyer-Vernet, M. Moncuquet, S. Hoang (1998) Solar wind radial and
747 latitudinal structure of electron density and core temperature from Ulysses thermal
748 noise spectroscopy, *J. Geophys. Res.*, *103*, 1969-1979.
- 749 Issautier, K., N. Meyer-Vernet, M. Moncuquet, S. Hoang, D. J. McComas (1999) Quasi-
750 thermal noise in a drifting plasma: Theory and application to solar wind diagnostic on

- 751 Ulysses, *J. Geophys. Res.*, *104*, 6691-6704.
- 752 Issautier, K., R. M. Skoug, J. T. Gosling, S. P. Gary, D. J. McComas (2001) Solar wind
753 plasma parameters on Ulysses: Detailed comparison between the URAP and SWOOPS
754 experiments, *J. Geophys. Res.*, *106*, 15665-15676.
- 755 Issautier, K., C. Perche, S. Hoang, C. Lacombe, M. Maksimovic, J.-L. Bougeret, S. Salem
756 (2005) Solar wind electron density and temperature over solar cycle 23: Thermal noise
757 measurements on Wind, *Adv. Space Res.*, *35*, 2141-2146.
- 758 Issautier, K., G. Le Chat, N. Meyer-Vernet, M. Moncuquet, S. Hoang, R. J. MacDowall,
759 D. J. McComas (2008) Electron properties of high-speed solar wind from polar coronal
760 holes obtained by Ulysses thermal noise spectroscopy: Not so dense, not so hot, *Geophys.*
761 *Res. Lett.*, *35*, CiteID L19101.
- 762 Kawasaki, K., S. Inoue, E. Ewang, K. Toyoda, M. Cho (2016), Measurement of elec-
763 tron emission yield by electrons and photons for space aged material, in *Proceed. 14th*
764 *Spacecraft Charging Technology Conf.*, eds. Hilgers et al., ESA/ESTEC, Noordwijk, NL.
- 765 Knoll, R., G. Epstein, S. Hoang, G. Huntzinger, J. L. Steinberg, J. Fainberg, F. Grena,
766 R. G. Stone, S. R. Mosier (1978) The 3-dimensional radio mapping experiment /SBH/
767 on ISEE-C, *IEEE Trans.*, *GE-16*, 199-204.
- 768 Laframboise, J. G. (1966) Theory of spherical and cylindrical Langmuir probes in a colli-
769 sionless Maxwellian plasma at rest, *Report 100*, Institute of Aerospace Studies, Univer-
770 sity of Toronto, Canada.
- 771 Lai, S. T., E. Murad, W. J. McNeil (2002) Hazards of hypervelocity impacts on spacecraft,
772 *J. Spacecraft Rockets* *39* 106–114.

- 773 Le Chat, G., K. Issautier, N. Meyer-Vernet, I. Zouganelis, M. Maksimovic, M. Moncuquet
774 (2009) Quasi-thermal noise in space plasma: “kappa” distributions, *Physics of Plasmas*,
775 *16*, 102903-102903-6.
- 776 Le Chat, G., K. Issautier, N. Meyer-Vernet, S. Hoang (2011) Large-Scale Variation of
777 SolarWind Electron Properties from Quasi-Thermal Noise Spectroscopy: Ulysses Mea-
778 surements, *Solar Phys.*, *271*, 141–148.
- 779 Lund, E. J., J. LaBelle, R. A. Treuman (1994) On quasi-thermal fluctuations near the
780 plasma frequency in the outer plasmasphere: A case study, *J. Geophys. Res.*, *99*, 23,651-
781 23,660.
- 782 Maksimovic, M., S. Hoang, N. Meyer-Vernet, M. Moncuquet, J.-L. Bougeret, J. L Phillips
783 and P. Canu (1995) Solar wind electron parameters from quasithermal noise spec-
784 troscopy and comparison with other measurements on Ulysses, *J. Geophys. Res.*, *100*,
785 19881–19891.
- 786 Maksimovic, M., K. Issautier, N. Meyer-Vernet, C. Perche, M. Moncuquet, I. Zouganelis,
787 S. D. Bale, N. Vilmer, J.-L. Bougeret (2005), Solar wind electron temperature and
788 density measurements on the Solar Orbiter with thermal noise spectroscopy, *Adv. Space*
789 *Res.*, *36*, 1471-1473.
- 790 Mann, I., N. Meyer-Vernet, A. Czechowski (2014), Dust in the planetary system: Dust
791 interactions in space plasmas of the solar system, *Physics Reports*, *536*, 1-39.
- 792 Martinovic, M. M., A. Zaslavsky, M. Maksimovic, S. Segan (2017) Electrostatic thermal
793 noise in a weakly ionized collisional plasma, *Radio Sci.*, *52*, 70-77.
- 794 Marsch, E., (2006), Kinetic physics of the solar corona and solar wind, *Living Rev. Solar*
795 *Phys.*, *3*, 1.

- 796 McBride, N. and J. A. M. McDonnell, (1999), Meteoroid impacts on spacecraft: Sporadics,
797 streams, and the 1999 Leonids, *Planet. Space Sci.* *47*, 1005–1013.
- 798 Meuris, P., N. Meyer-Vernet and J. F. Lemaire (1996) The detection of dust grains by a
799 wire dipole antenna: the radio dust analyzer, *J. Geophys. Res.*, *101*, 24,471-24,477.
- 800 Meyer, P., N. Vernet (1974) The impedance of a short antenna in a warm magnetoplasma,
801 *Radio Science*, *9*, 409416.
- 802 Meyer, P., N. Vernet (1975) The impedance of a dipole antenna in the ionosphere, 2,
803 Comparison with theory, *Radio Science*, *10*, 529536.
- 804 Meyer-Vernet, N., P. Meyer, C. Perche (1977) Noncollisional losses in an inhomogeneous
805 plasma, *Phys. Fluids*, *20*, 536-537.
- 806 Meyer-Vernet, N., P. Meyer, C. Perche (1978) Losses due to the inhomogeneous sheath
807 surrounding an antenna in a plasma, *Radio Science*, *13*, 69-73.
- 808 Meyer-Vernet, N. (1979) On natural noises detected by antennas in plasmas, *J. Geophys.*
809 *Res.*, *84*, 5373–5377.
- 810 Meyer-Vernet, N. et al. (1986a), Plasma diagnosis from thermal noise and limits on dust
811 flux or mass in Comet Giacobini-Zinner, *Science*, *232*, 370374.
- 812 Meyer-Vernet, N. et al. (1986b), Physical parameters for hot and cold electron populations
813 in Comet Giacobini-Zinner with the ICE radio experiment, *Geophys. Res. Lett.*, *13*, 279-
814 282.
- 815 Meyer-Vernet, N. and C. Perche (1989) Toolkit for antennae and thermal noise near the
816 plasma frequency, *J. Geophys. Res.*, *94*, 2405-2415.
- 817 Meyer-Vernet, N., S. Hoang, M. Moncuquet (1993) Bernstein waves in the Io plasma torus:
818 A novel kind of electron temperature sensor, *J. Geophys. Res.*, *98*, 21,163-21,176.

- 819 Meyer-Vernet, N. (1993), Aspects of Debye shielding, *Am. J. Phys.*, *61*, 249-257.
- 820 Meyer-Vernet, N. (1994) On the thermal noise” temperature”in an anisotropic plasma,
821 *Geophys. Res. Lett.*, *21*, 397–400.
- 822 Meyer-Vernet, N., S. Hoang, K. Issautier, M. Maksimovic, R. Manning, M. Moncuquet,
823 R. Stone (1998), Measuring plasma parameters with thermal noise spectroscopy, in
824 *Measurement techniques in space plasmas: fields, Geophys. Monograph Ser.*, vol. 103,
825 edited by R. Pfaff et al., AGU, Washington DC., pp. 205-210.
- 826 Meyer-Vernet, N., S. Hoang, K. Issautier, M. Maksimovic, M. Moncuquet, G. Marcos
827 (2000), Plasma thermal noise: the long wavelength radio limit, in *Radioastronomy at*
828 *long wavelengths, Geophys. Monograph Ser.*, vol. 119, edited by R. G. Stone et al., AGU,
829 Washington DC., pp. 67-74.
- 830 Meyer-Vernet, N. (2001) Large scale structure of planetary environments: the importance
831 of not being Maxwellian, *Planet. Space Sci.*, *49*, 247-260.
- 832 Meyer-Vernet (2013), On the charge of nanograins in cold environments and Enceladus
833 dust, *Icarus*, *226*, 583-590.
- 834 Meyer-Vernet, N., M. Moncuquet, K. Issautier, and P. Schippers (2016), Frequency range
835 of dust detection in space with radio and plasma wave receivers: Theory and application
836 to interplanetary nanodust impacts on Cassini, *J. Geophys. Res. Space Physics*, *121*
837 doi:10.1002/2016JA023081.
- 838 Moncuquet, M., N. Meyer-Vernet, S. Hoang (1995), Dispersion of electrostatic waves in the
839 Io plasma torus and derived electron temperature, *J. Geophys. Res.*, *100*, 21697-21708.
- 840 Moncuquet, M., N. Meyer-Vernet, S. Hoang, R. J. Forsyth, P. Canu (1997), Detection of
841 Bernstein wave forbidden bands in the Jovian magnetosphere: A new way to measure

- 842 the electron density, *J. Geophys. Res.*, *102*, 2373-2380.
- 843 Moncuquet, M., A. Lecacheux, N. Meyer-Vernet, B. Cecconi, W. S. Kurth (2005), Quasi
844 thermal noise spectroscopy in the inner magnetosphere of Saturn with Cassini/RPWS:
845 Electron temperatures and density, *Geophys. Res. Lett.*, *32*, CiteID L20S02.
- 846 Moncuquet, M. et al. (2006a), The radio waves and thermal electrostatic noise spec-
847 troscopy (SORBET) experiment on BEPICOLOMBO/MMO/PWI: Scientific objectives
848 and performance, *Adv. Space Res.*, *38*, 680-685.
- 849 M. Moncuquet, N. Meyer-Vernet, A. Lecacheux, B. Cecconi, and W. S. Kurth (2006b),
850 Quasi Thermal Noise in Bernstein Waves at Saturn. In H. O. Rucker, W. Kurth, and
851 G. Mann, editors, Planetary Radio Emissions VI, p. 93.
- 852 Nicholls, D. C., M. A. Dopita, R. S. Sutherland (2012), Resolving the electron temperature
853 discrepancies in HII regions and planetary nebulae: κ -distributed electrons, *Astrophys.*
854 *J.*, *752*, 148.
- 855 Nyquist, H. (1928), Thermal agitation of electric charge in conductors, *Phys. Rev.*, *23*,
856 110.
- 857 Ockham, W. of (1324), *Summa Totius Logicae*, *i. 12*.
- 858 Rostoker, N. (1961), Fluctuations of a plasma, *Nucl. Fusion*, *1*, 101-120.
- 859 Saint-Hilaire, P. et al. (2014), The Cubesat Radio Experiment (CURE) and Beyond:
860 Cubesat-based Low Frequency Radio Interferometry, *AGU Fall meeting*, abstract
861 SH53B-4231.
- 862 Salem, C., J.-M. Bosqued, D. E. Larson, A. Mangeney, M. Maksimovic, C. Perche, R. P.
863 Lin, J.-L. Bougeret (2001), Determination of accurate solar wind electron parameters
864 using particle detectors and radio wave receivers, *J. Geophys. Res.*, *106*, 21701-21717.

- 865 Schiff, M., L. (1970), Impedance of a short dipole antenna in a warm isotropic plasma,
866 *Radio Sci.*, *5*, 1489-1496.
- 867 Schippers, P., M. Moncuquet, N. Meyer-Vernet, A. Lecacheux (2013), Core electron tem-
868 perature and density in the innermost Saturn's magnetosphere from HF power spectra
869 analysis on Cassini, *J. Geophys. Res.*, *118*, 7170-7180.
- 870 Scudder, J., S. Olbert (1979), A theory of local and global processes which affect solar
871 wind electrons: The origin of typical 1 AU velocity distribution functions – Steady state
872 theory, *J. Geophys. Res.*, *84*, 2755.
- 873 Scudder, J. D., H. Karimabadi (2013), Ubiquitous non-thermals in astrophysical plasmas:
874 Restating the difficulty of maintaining Maxwellians, *Astrophys. J.*, *770*, 26.
- 875 Sentman, D. D. (1982), Thermal fluctuations and the diffuse electrostatic emissions, *J.*
876 *Geophys. Res.*, *87*, 1455-1472.
- 877 Shukla, P. K. and A. A. Mamun (2002) Introduction to dusty plasma physics, IOP Pub-
878 lishing Ltd, Bristol.
- 879 Sitenko, A. G. (1967) Electromagnetic fluctuations in plasmas, Academic Press, San
880 Diego, USA.
- 881 Swartwout, M. (2013), The First One Hundred CubeSats: A Statistical Look, *JoSS*, *2*,
882 213-233.
- 883 Tong, Y., M. Pulupa, C. S. Salem, S. D. Bale (2015), Investigating WIND quasi-thermal
884 noise spectra between the ion and the electron plasma frequency, *AGU Fall Meeting*
885 *2015*.
- 886 Vasyliunas, V. M. (1968), A survey of low-energy electrons in the evening sector of the
887 magnetosphere with Ogo 1 and Ogo 3, *J. Geophys. Res.*, *73*, 2839-2885.

- 888 Verheest, F. (1996), Waves and instabilities in dusty space plasmas, *Space Sci. Rev.*, *77*,
889 267-302.
- 890 Wang, L. et al. (2012), Quiet-time interplanetary $\simeq 2 - 20$ keV superhalo electrons at
891 solar minimum, *Astrophys. J. Lett.*, *753*, L23.
- 892 Whipple, E. C. (1981), Potentials of surfaces in space, *Rep. Prog. Phys.*, *44*, 1197–1250.
- 893 Yoon, P. H. (2014), Electron kappa distribution and quasi-thermal noise, *J. Geophys.*
894 *Res.*, *119*, 7074–7087.
- 895 Yoon, P. H., S. Kim, G. S. Choe, Y.-J. Moon (2016), Revised model of the steady-state
896 solar wind halo electron velocity distribution function, *Astrophys. J.*, *826*, 204.
- 897 Yoon, P. H., J. Hwang, D. K. Shin (2017), Upper hybrid waves and energetic electrons in
898 the radiation belt, *J. Geophys. Res.*, *122*, 5365-5376.
- 899 Zouganelis, I., Maksimovic, M., Meyer-Vernet, N., Issautier, K., Moncuquet, M., Bale, S.
900 D. (2007), Implementation of the thermal noise spectroscopy on Solar Orbiter, in *Proceed.*
901 *2nd Solar Orbiter workshop*, ESA-SP 641, eds. Marsch, E., Tsinganos, K., Marsden, R.,
902 Conroy, L., Noordwijk, Netherlands.
- 903 Zouganelis, I. (2008), Measuring suprathermal electron parameters in space plasmas: Im-
904 plementation of the quasi-thermal noise spectroscopy with kappa distributions using
905 in situ Ulysses/URAP radio measurements in the solar wind, *J. Geophys. Res.*, *113*,
906 A08111, doi:10.1029/2007JA012979.
- 907 Zouganelis, I. et al. (2010), Measurements of stray antenna capacitance in the
908 STEREO/WAVES instrument: Comparison of the measured voltage spectrum with an
909 antenna electron shot noise model, *Radio Sci.*, *45*, RS1005, doi:10.1029/2009RS004194.

Table 1. Properties of wire dipole antennas (length L of each element, radius a , and dipole stray capacitance^b) used for QTN on ISEE 3-ICE/3D Radio Mapping, Ulysses/URAP^a, WIND/WAVES, Cassini/RPWS, MMO-BepiColombo/PWI-WPT, Solar Orbiter (SO)/RPW and Parker Solar Probe (PSP)/FIELDS, and average Debye length in the solar wind at respectively 1 AU (ISEE 3, Ulysses, Wind), 0.3 AU (representative for Bepi-Colombo and SO), $10 R_s$ (closest heliocentric distance of PSP), and in Saturn’s magnetosphere at Enceladus’ orbit (explored by Cassini).

Property	ISEE 3	Ulysses	WIND	Cassini	BepiColombo	SO	PSP
L (m)	45	35	50 ^c	10	15	6.5	2
a (mm)	0.2	1.1	0.2	14.3	0.21	14.2	1.59
C_b (pF)	45	57	20	55	50? ^b	? ^b	35 ^b
L_D (m)	10	10	10	1	5	5	0.8

^a For Ulysses antennas (tapes of length L , width 5 mm and thickness 0.04 mm), the radius is that of the cylinder having the same capacitance.

^b The base capacitance can be measured accurately only after the antennas have been extended on the spacecraft in space.

^c The length indicated holds at the times when Figs 6 and 7 were acquired, i.e. before the antenna wires were broken by dust impacts.

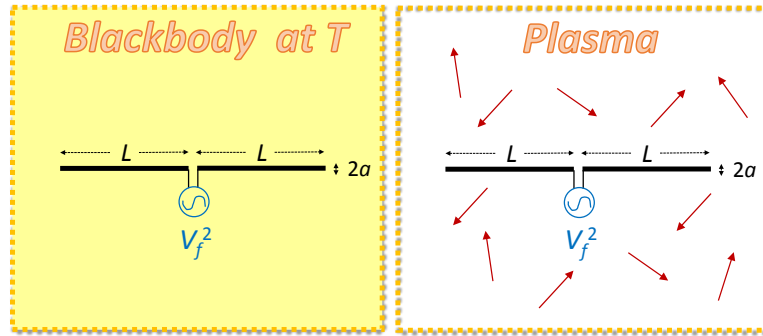


Figure 1. Simple electric antenna (two aligned wires of length L and radius a) immersed in blackbody radiation (left) and in a plasma (right). When $L_D \ll L \ll \lambda = c/f$ (L_D is the plasma Debye length, c the speed of light and f the frequency), the antenna resistances are respectively $R_{EM} = 2\pi f^2 L^2 / (3\epsilon_0 c^3)$ (left) and $R_P \simeq (2/\pi)^{-1/2} (8\pi\epsilon_0 f_p L)^{-1}$ just below the plasma frequency f_p peak, and $R_P \simeq f_p^2 (4\pi\epsilon_0 f^3 L)^{-1}$ for $f \gg f_p$ (right).

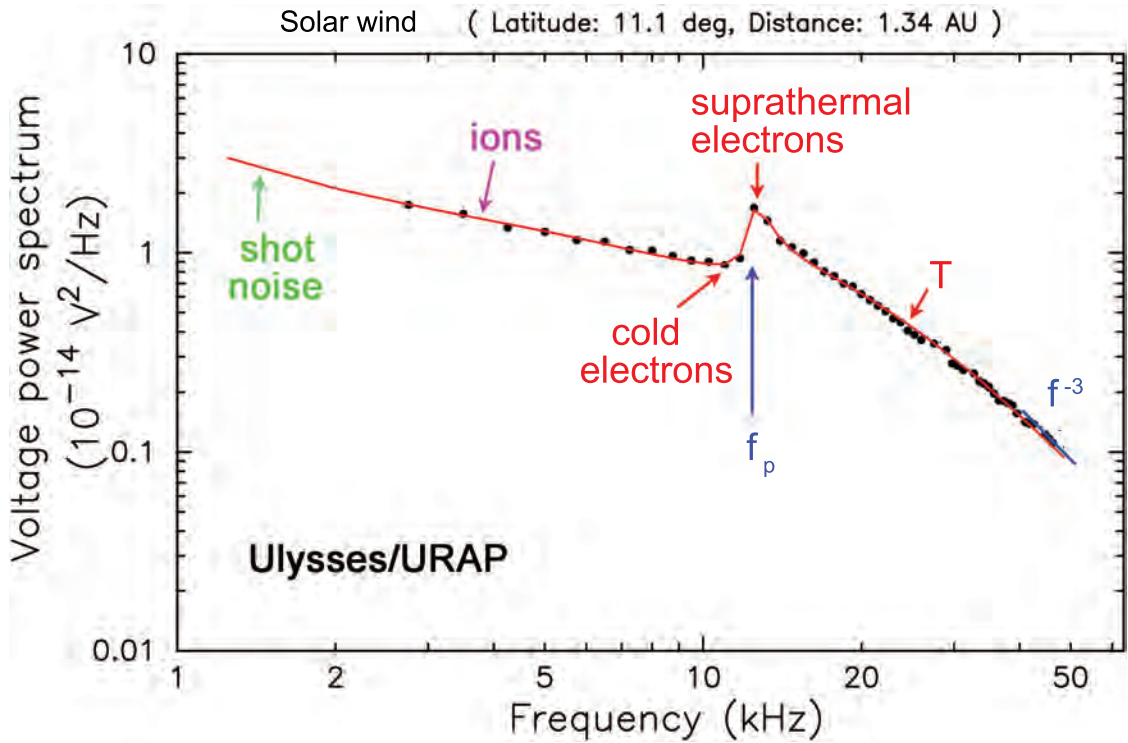


Figure 2. Example of QTN spectrum (V_r^2 , measured at the receiver's ports) with a wire dipole antenna in a weakly magnetized plasma (Ulysses/URAP data in the solar wind). The main plasma parameters that can be deduced are indicated. Fitted electron parameters, assuming an electron velocity distribution made of a sum of a cold and a hot maxwellian are: $n = 1.8 \times 10^6 \text{ m}^{-3}$, $T_c = 1.3 \times 10^5 \text{ K}$, $T_h/T_c = 8$, $n_h/n_c = 0.04$ (with an accuracy of 1% on n and 7 % on T). Note that for a quick diagnostics, one can deduce the total electron density from the f_p peak, the cold electron temperature from (41) and the kinetic electron temperature from (46), using V_f^2 calculated via (44) with C_a from (43) and (47) at respectively low and high frequencies.

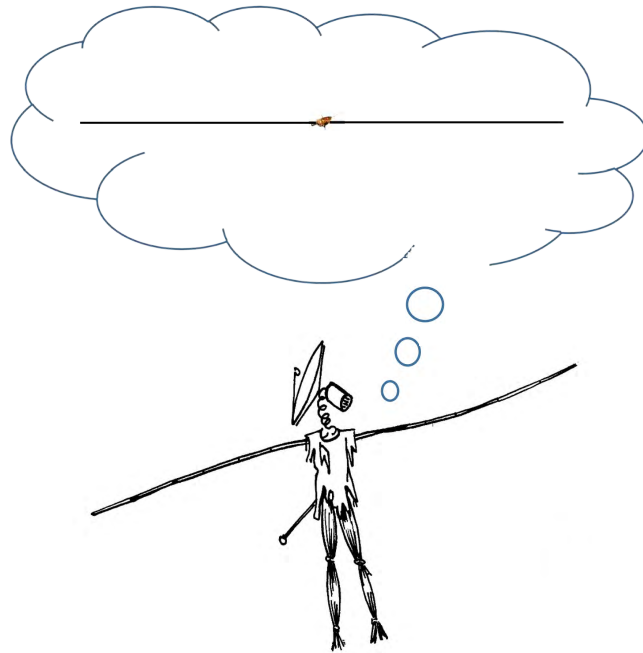


Figure 3. Unfortunately, the strawman payload of the space agencies (bottom) is different from the ideal case for QTN spectroscopy (top), when the spacecraft size is much smaller than the antenna length and the antennas are thin, symmetrical and unbiased - as for ISEE 3 and Ulysses (shown to scale between the antenna wires). Drawing by François Meyer.

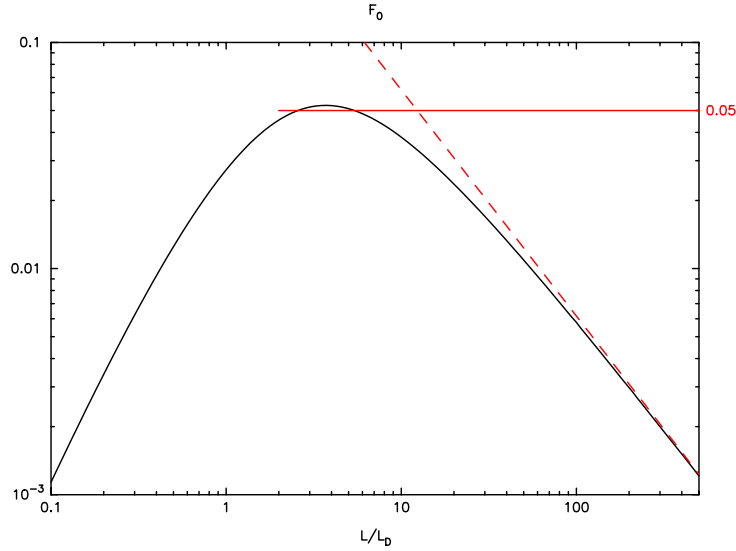


Figure 4. Function $F_0(L/L_D)$ given by (37). Multiplying F_0 by the factor $2^{7/2}(mk_B)^{1/2}/(\pi^{3/2}\epsilon_0) \simeq 8.14 \times 10^{-16}$ yields the QTN plateau V_f^2 normalized to $[T_{-2}/T_{-1}^{1/2}]$, close to the square root of the “cold” temperature (in $\text{V}^2\text{Hz}^{-1}\text{K}^{-1/2}$) (see Eq.(36)). The dashed red line shows the approximation (38) (valid for very long antennas); the solid red line shows the approximation $F_0 \simeq 0.05$ (valid for intermediate lengths).

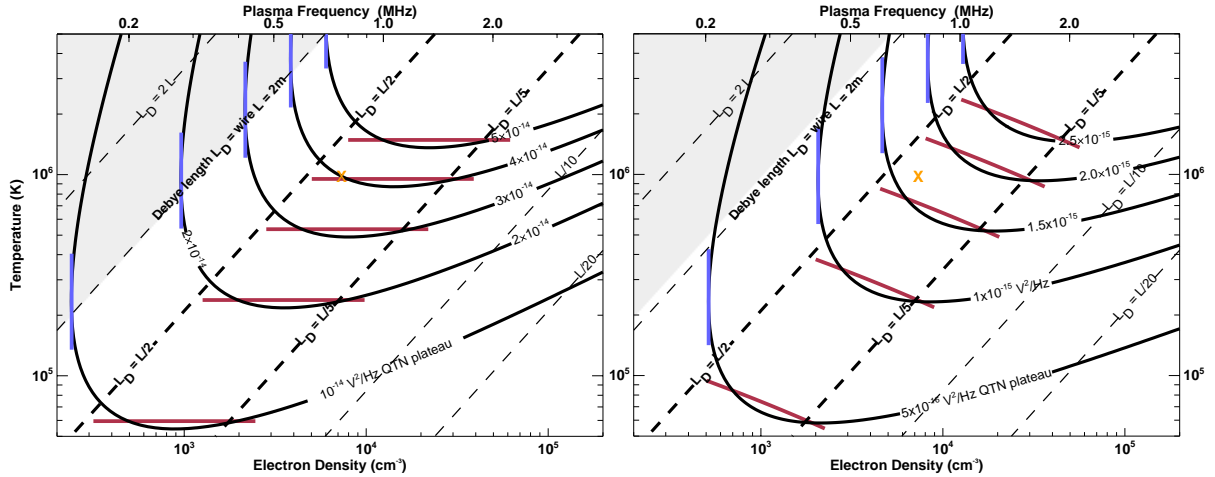


Figure 5. QTN plateau level in V^2Hz^{-1} with the wire dipole antenna of PSP/FIELDS ($L = 2$ m) in a density/temperature plane, with the approximation (40) superimposed as red bars. The power is calculated at both the antenna ports (left, from (36)) and the receiver ports (right, deduced via (7)). The variation in antenna capacitance (43) with L_D makes V_r^2/V_f^2 vary with the electron density, so that the horizontal lines (left) become inclined (right). The orange cross sketches the density and temperature expected for PSP near perihelion. The range $L/L_D < 1$, in which QTN spectroscopy become ineffective is shown in grey; the blue vertical lines show the regions in which the QTN plateau level becomes weakly dependent of temperature, making this derivation difficult.

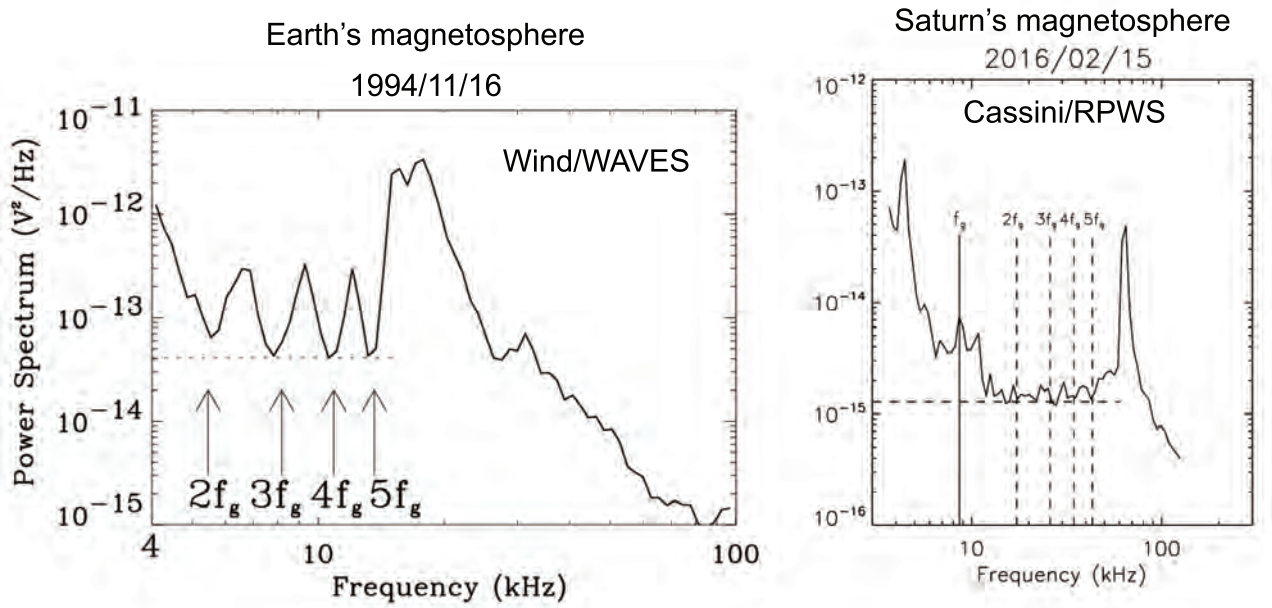


Figure 6. Two examples of quasi-thermal noise spectra (V_r^2 , measured at the receiver ports) in magnetized plasmas, showing a plateau of minima (dashed horizontal line) at the gyroharmonics nf_g . Left-hand side: Wind/WAVES data in the Earth's magnetosphere at 8 Earth's radii. Right-hand side: Cassini/RPWS data in Saturn's magnetosphere at 4 Saturn's radii.

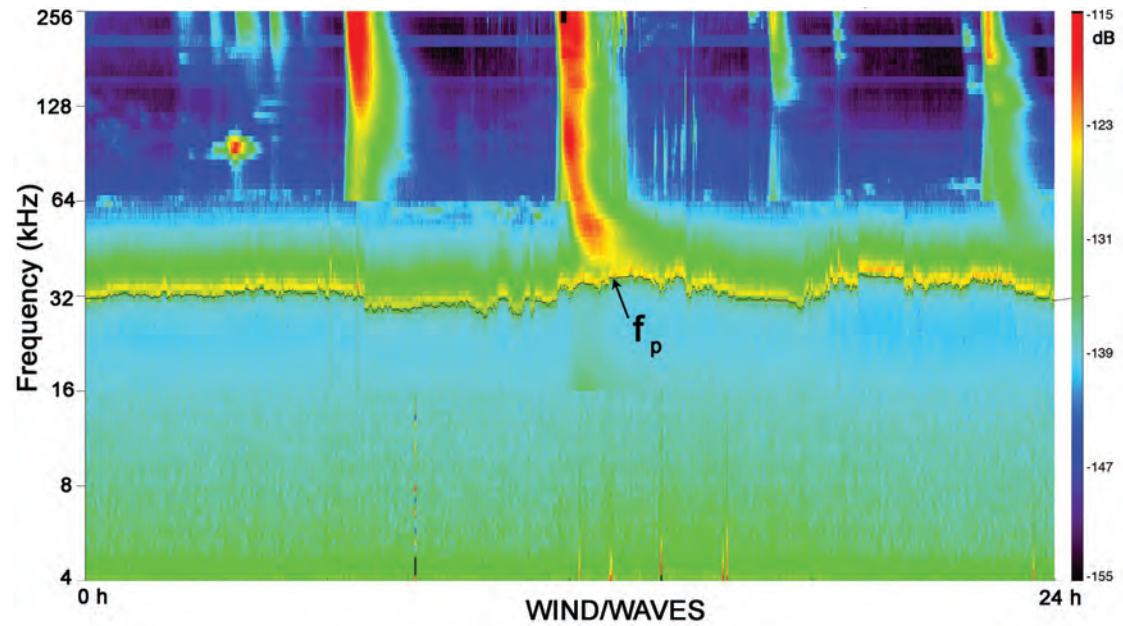


Figure 7. Radio spectrogram from WIND/WAVES acquired on 5 November 1997 in the solar wind, showing solar radioemissions perturbing the plasma QTN above the plasma frequency, whereas the f_p line and QTN plateau are not perturbed. The data are plotted as frequency versus time, with the relative intensity coded as indicated in the color bar.